MARTIN MARIETTA ENERGY SYSTEMS LIBRARIES

3 4456 0350438 5

CENTRAL RESEARCH LIBRARY
DOCUMENT COLLECTION

ORNL-2201
cy. 4

ORNL-2201
Criticality Studies

TWO BERYLLIUM-MODERATED CRITICAL ASSEMBLIES

E. L. Zimmerman

OAK RIDGE NATIONAL LABORATORY
operated by
UNION CARBIDE CORPORATION
for the
U.S. ATOMIC ENERGY COMMISSION

Printed in USA. Price 1.75 cents. Available from the

Office of Technical Services
U. S. Department of Commerce
Washington 25, D. C.

LEGAL NOTICE

This report was prepared as an account of Government sponsored work. Neither the United States, nor the Commission, nor any person acting on behalf of the Commission:

A. Makes any warranty or representation, express or implied, with respect to the accuracy, completeness, or usefulness of the information contained in this report, or that the use of any information, apparatus, method, or process disclosed in this report may not infringe privately owned rights; or

B. Assumes any liabilities with respect to the use of, or for damages resulting from the use of any information, apparatus, method, or process disclosed in this report.

As used in the above, "person acting on behalf of the Commission" includes any employee or contractor of the Commission to the extent that such employee or contractor prepares, handles or distributes, or provides access to, any information pursuant to his employment or contract with the Commission.

ORNL-2201
Criticality Studies

Contract No. W-7405-eng-26

Neutron Physics Division

TWO BERYLLIUM-MODERATED CRITICAL ASSEMBLIES

E. L. Zimmerman*

DATE ISSUED

OCT 6 1958

OAK RIDGE NATIONAL LABORATORY
Oak Ridge, Tennessee
operated by
UNION CARBIDE CORPORATION
for the
U.S. ATOMIC ENERGY COMMISSION

*Present address: Nuclear Development Corporation of Americ
White Plains, New York

MARTIN MARIETTA ENERGY SYSTEMS LIBRARIES
3 4456 0350438 5

ABSTRACT

Two unreflected critical assemblies using beryllium as the moderator and 93.4% enriched uranium metal as the fuel were built to provide a basis for the evaluation of certain reactor calculational procedures. Control and safety rods of the core-element-removal type were used in order that the final assemblies would not be complicated by strong absorber rods. In the first assembly (CA-1), which had outside dimensions of 21.0 x 21.0 x 23.3 in., the 0.01-in.-thick uranium disks were separated by 1-in.-thick blocks of beryllium, which gave a $Be:U^{235}$ atomic ratio of 390 and a fuel loading of 18.08 kg of U^{235}. The extrapolated value of k_{eff} for the system was 1.0054. In the second assembly (CA-18), which had outside dimensions of 24.0 x 28.4 x 24.1 in., the fuel disks were separated by 4-in.-thick blocks of beryllium, which gave a $Be:U^{235}$ ratio of 1560 and a fuel loading of 7.65 kg of U^{235}. For this assembly the extrapolated k_{eff} value was 1.0020. The observed uranium cadmium fractions in the two assemblies were 0.46 and 0.86, respectively.

A number of multigroup calculations were made to evaluate the effects of various corrections and assumptions. It was concluded that the calculated neutron multiplication is very sensitive to the competition between leakage and slowing down at high energies, a range where fundamental data are uncertain. Without resolving the detailed neutron behaviors in this range, a reasonable selection of data within experimental uncertainties will give satisfactory values for such quantities as critical size.

PREFACE AND ACKNOWLEDGEMENTS

During the late 1940's both the Oak Ridge National Laboratory and the Nuclear Energy Propulsion Aircraft Division of the Fairchild Engine and Airplane Corporation in Oak Ridge became interested in performing critical experiments which could be correlated with reactor calculations. Accordingly, a critical experiments facility was constructed and equipped, and plans were made for the two groups to jointly build and operate a simple unreflected beryllium-moderated assembly. The assembly, designated as CA-1, became critical in the early part of 1951. Shortly after the inauguration of the program the NEPA project was terminated and its personnel dispersed, leaving the experimental program incomplete. The Critical Experiments Laboratory continued as an ORNL facility and, after a brief interruption, the experimental program with CA-1 was resumed. Although no complete report of the experiments was ever prepared, some of the results were publicized through private communications, and the discrepancy between the predicted and actual critical size of the assembly gave rise to rather widespread interest. Several attempts, both theoretical and experimental, were made to determine the source of the disagreement, and an interest on the part of ORNL staff members in resolving this problem as well as other inconsistencies associated with the calibration of CA-1 led to the construction in 1954 of a second beryllium-moderated critical assembly, CA-18. Additional calculations were then performed by the author for both assemblies. This report describes the two experiments and presents the calculations. It is to be pointed out that these calculations were completed in 1954 using the best cross-section data available at that time, and the effect of using more recent values has not been investigated.

The success of the two experimental programs is the result of the cooperative efforts of many persons. The equipment and most of the material necessary for the first assembly (CA-1) were procured by the NEPA Group, and the experiment itself was performed with their assistance. The members of this group were:

	Present Address
J. Frank Coneybear, Dan Weinberg and Henry Kroeger	ASTRA Associates, Milford, Connecticut
Frank Bly	Lockheed Aircraft Company, Marietta, Ga.
A. O. Mooneyham and E. V. Haake	Convair, Fort Worth, Texas
J. A. Hunter	The Martin Company, Baltimore, Maryland
Fred Pressey	Grenada, British West Indies

The ORNL staff members who assisted in the performance of one or both experiments were:

K. W. Downes	Brookhaven National Laboratory, Upton, N.Y.
J. W. Noaks, on leave from Pratt and Whitney Aircraft	Alco Products, Inc., Schenectady, N.Y.
D. V. P. Williams	Babcock and Wilcox, Lynchburg, Virginia
A. D. Callihan, J. H. Marable, E. R. Rohrer and Dunlap Scott	Oak Ridge National Laboratory

Special appreciation is extended to Dr. Callihan for his help throughout both experiments and during the preparation of this report.

TABLE OF CONTENTS

		Page No.
	Abstract	iii
	Preface and Acknowledgements	iv
	Introduction	1
I.	Description of the Assemblies	2
II.	Experimental Measurements	7
	Measurements with CA-1	7
	Initial Approach to Criticality	7
	Control Rod Calibration	7
	Reactivity Measurements	7
	Miscellaneous Measurements	10
	Measurements with CA-18	10
	Initial Approach to Criticality	10
	Control Rod Calibration	10
	Foil Exposures	13
	Reactivity Measurements	17
III.	Multigroup Calculations	25
	General Calculation Procedure	25
	Variations in Calculations	25
	Uranium Self-Shielding Corrections	25
	Elastic Versus Inelastic Scattering in U^{235}	28
	Isotropic Versus Anisotropic Scattering in Beryllium	28
	Nuclear Reactions in Beryllium	30
	Methods of Computing Neutron Slowing-Down Density	30
	Correction for Effect of External Aluminum Grid	30
	Results of the Multigroup Calculations	31
	Comparison of Present Calculations for CA-1 with Previous Calculations	37
IV.	Conclusions	38
App. A.	Calculation of the Reactivity Value of a Beryllium Layer on Top of CA-18	40
App. B.	Multigroup Formulation	42
App. C.	Source Distribution and Corresponding Cross-Section Data for the Reactor Materials	44
App. D.	Calculations of Self-Shielding Corrections	45

Table of Contents (cont.)

Page No.

App. E. Calculations of ξ for Anisotropic Scattering 50

App. F. Correction for External Aluminum Grid 52

App. G. List of Figures 56

App. H. List of Tables 58

INTRODUCTION

Multigroup reactor calculation methods were first used in Oak Ridge in 1950 by the NEPA and ORNL Physics Groups, at which time the critical size of an unreflected beryllium-moderated reactor was calculated.[1] In order to experimentally check the validity of the calculational method, a critical assembly was built in the NEPA-ORNL Critical Experiments Facility.[2] This assembly, designated as CA-1, was of the simplest possible geometry, approximating a bare cube. It had a regular lattice of 10-mil-thick enriched uranium metal fuel disks separated by 1-in.-thick blocks of beryllium metal. Besides the ease of construction, such an assembly had the advantage of permitting relatively simple corrections for fuel heterogeneity, and the more complicated calculations necessary for a reflected system could be avoided.

CA-1 was first made critical February 4, 1951. The size of the assembly was roughly 27% less than had been predicted.[1,3] Therefore considerable experimental effort was directed toward finding possible experimental errors. Subsequently a number of calculational attempts were made[4-6] which resulted in more or less rationalizing the discrepancy between theory and experiment. In the spring of 1951 the NEPA project was terminated, resulting in the early curtailment of experiments on this critical assembly.

Until April, 1954, CA-1 remained the only simple beryllium-moderated critical assembly available for analysis. At that time a second assembly, designated as CA-18, was built similar to CA-1 except that the fuel spacing was changed from 1 to 4 in. It was recognized that an assembly having a higher uranium concentration than that of CA-1 would have been more desirable from the analytical standpoint, since the greatest uncertainties in cross-section data are in the high-energy range. However, the 4-in. spacing was chosen on the basis of ease of construction and the availability of materials and time.

Upon completion of CA-18 several multigroup calculations were performed and compared with the actual critical assemblies. These calculations for CA-1 were also compared with the earlier calculations. The purpose of this report is to describe the two critical assemblies in detail, to discuss the experimental measurements which were made in connection with them, and to evaluate various assumptions made in the multigroup calculations.*

---

1. A. O. Mooneyham, NEPA-1710 (1951) (Classified).
2. F. T. Bly et al., "NEPA Critical Experiment Facility," NEPA-1769 (1951).
3. A. O. Mooneyham, IC-51-2-7 (Supplement to NEPA-1710) (1951) (Classified).
4. G. M. Safanov, YF-10-45 (1951) (Classified).
5. D. K. Holmes, ORNL-1227, p. 64 (Classified).
6. C. B. Mills, ORNL-1493 (1953) (Classified).

* Calculations reported here were completed in 1954 using the best data available at that time. The effects of subsequent improvements in data have not been thoroughly investigated. However, the experimental results are still valid and will continue to serve as a comparison for subsequent calculation techniques.

I. DESCRIPTION OF THE ASSEMBLIES

The matrix into which the materials for both of the assemblies were placed was a 6-ft cube consisting of 3-in.-OD square 2S aluminum tubes, each having a wall thickness of 0.047 in. This matrix, which is shown in Fig. 1 for CA-1, was divided vertically into halves which could be separated by remote control. Fuel elements were placed in both halves and the assembly was completed by bringing them together.

Core elements consisted of 93.4% enriched, 2.860-in.-dia, 0.01-in.-thick uranium disks (average mass of U^{235} = 16.774 g) separated by one (CA-1) or four (CA-18) 1-in.-thick by 2-7/8 in. by 2-7/8 in. beryllium metal blocks of average density 1.86 g/cc. These were held together by 3/16-in.-dia aluminum skewers through 0.196-in.-dia center holes in the fuel disks and the beryllium blocks. The elements were designed to maintain a constant fuel spacing throughout the assembly.

The arrangements of the core elements in the aluminum grid for CA-1 and CA-18 are indicated in Figs. 2 and 3, respectively. Row 8 of CA-18 contained quarter-sized core elements. They were 1-7/16 in. square but otherwise had the same composition as the other elements.

Control and safety rods were similar to other core elements except that provision was made for remotely moving them within the assembly. The use of this type of control and safety devices permitted an assembly free of perturbing neutron absorbers. In order to give these elements more structural strength, stainless steel rather than aluminum skewers were used. The safety rods were inserted by compressed air, spring loaded and magnet held. All safety rod elements were inserted or withdrawn by means of a screw drive mechanism. One such element is shown displaced from its normal position in Fig. 1.

For CA-18 a simple servo control system was devised[7] which employed a 1X Brown "Electronic"* amplifier and a 27-rpm balancing motor arranged to insert or withdraw one of the core elements. This control element was located in cell K-13, as shown in Fig. 3. The input signal was derived from one of the neutron monitoring instruments in opposition to an adjustable demand potential supplied by a 1.5-v battery. The system was capable of changing the reactivity of the assembly at a maximum rate of 0.01%/sec, which was adequate to follow slow transients or to maintain stable operations.

A comparison of the physical compositions of the two assemblies is given in Table 1. For completeness the corresponding k_{eff} values are included. These values correspond to the regular assembly having the indicated fuel loadings extrapolated to the condition of all control rods fully inserted. Criticality in both assemblies was reached with one control rod slightly withdrawn. Each stainless steel volume fraction includes the stainless steel

---

7. M. E. Remley, Science 119, 29 (1954).
* Minneapolis-Honeywell Regulator Company, Philadelphia 44, Pa.

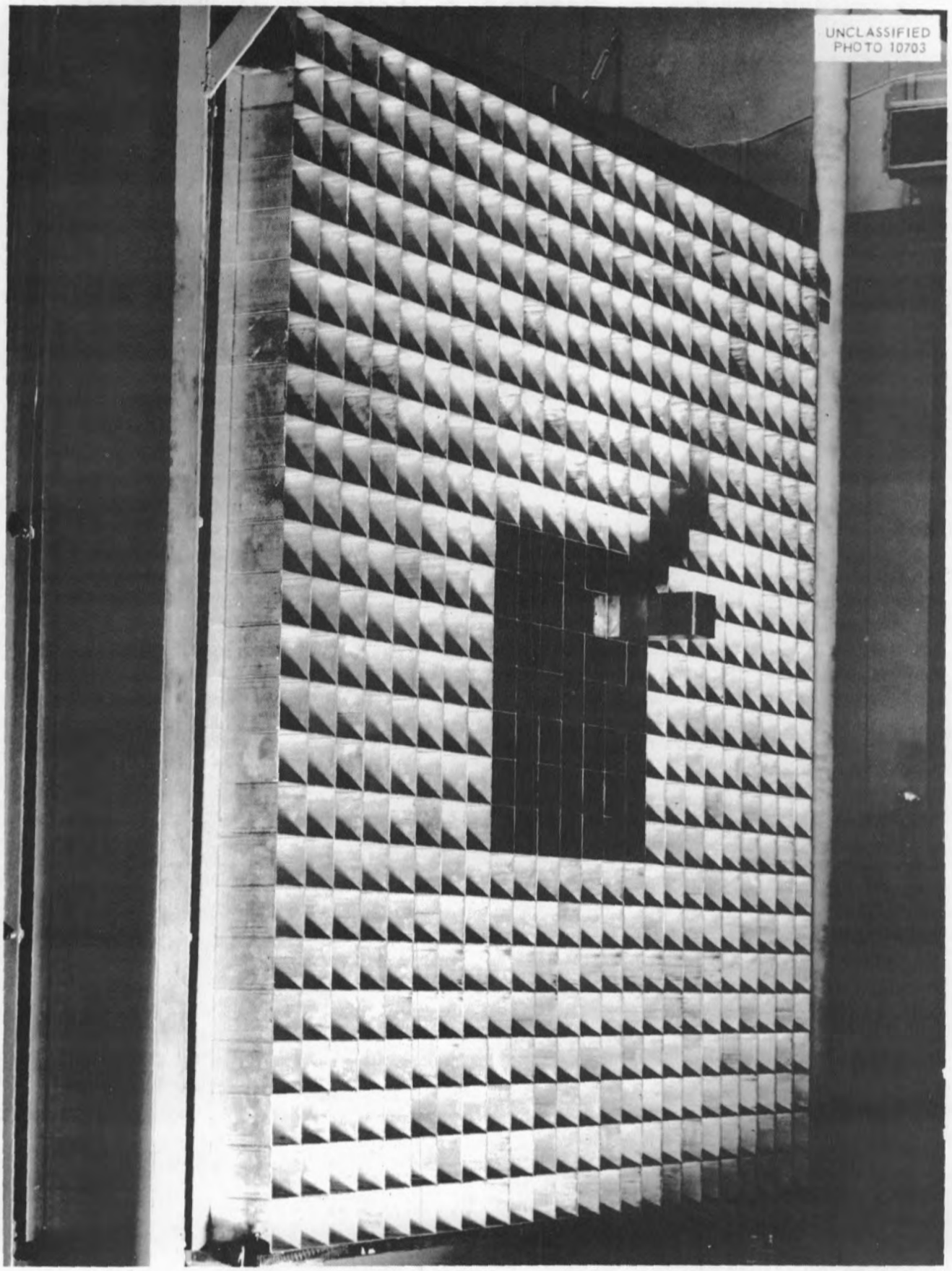

Fig. 1. Midplane of CA-1.

UNCLASSIFIED
ORNL-LR-DWG 14829

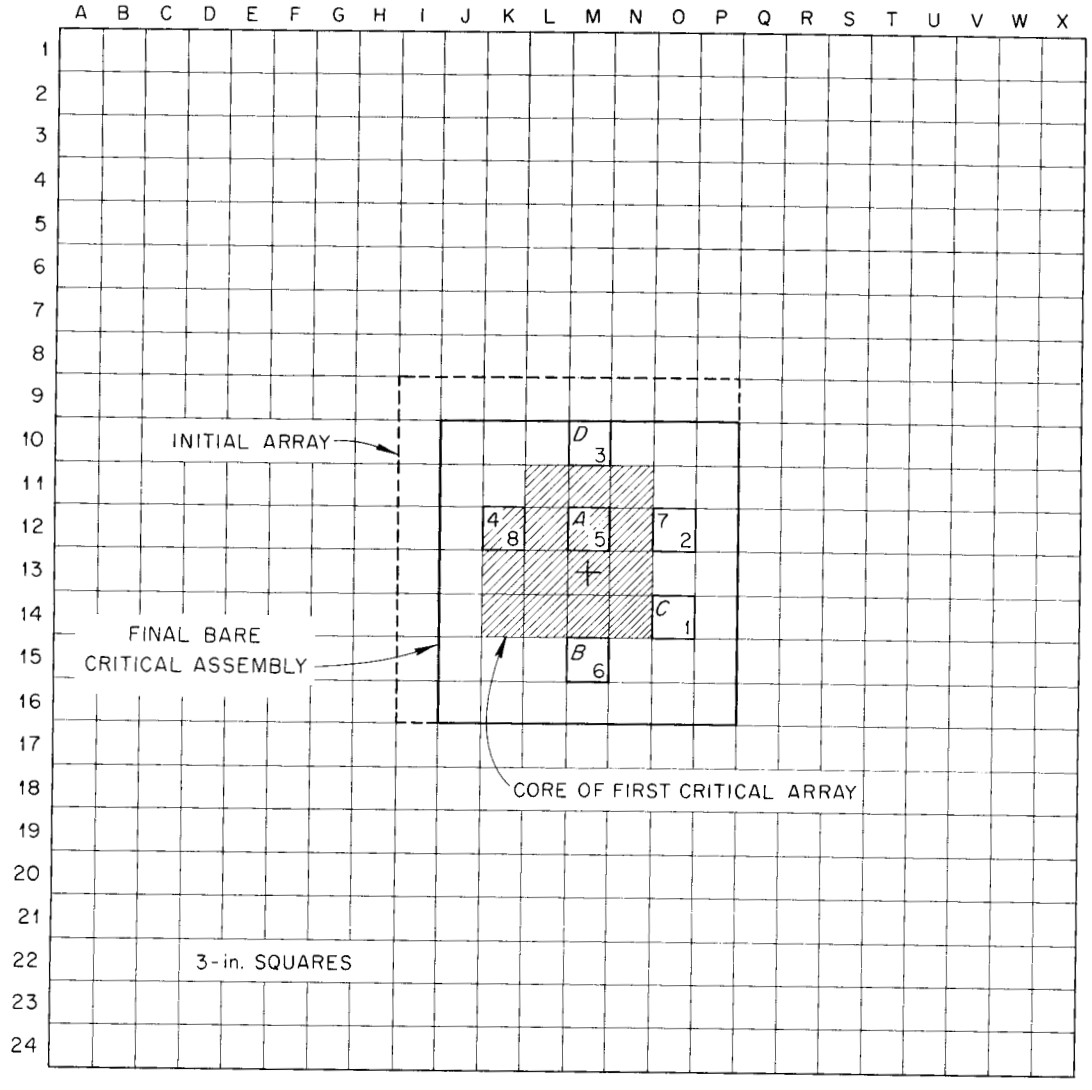

1, 2, 3, 4 = SAFETY RODS IN MOVABLE HALF
5, 6, 7, 8 = SAFETY RODS IN FIXED HALF

A, *B* = CONTROL RODS IN MOVABLE HALF
C, *D* = CONTROL RODS IN FIXED HALF

FUEL ELEMENT DETAIL

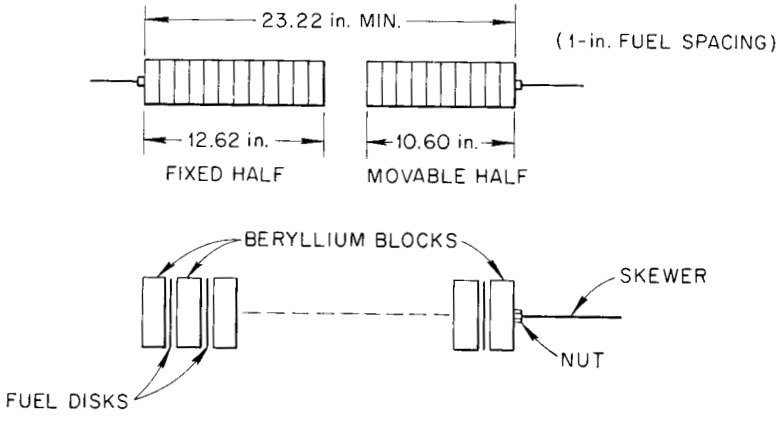

Fig. 2. Arrangement of Core Elements in CA-1 (Fixed Half Interface)

UNCLASSIFIED
ORNL-LR-DWG 14830

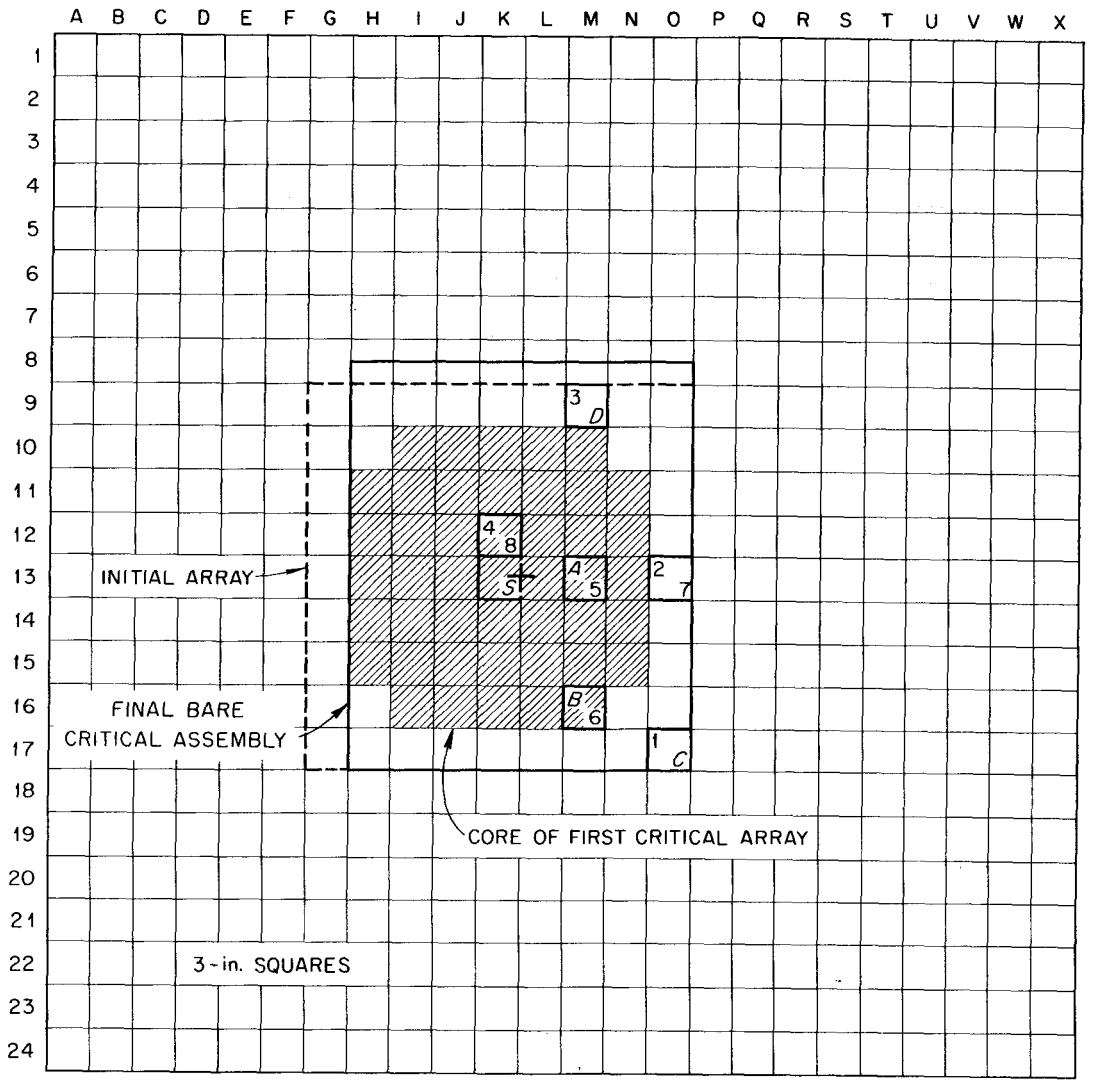

1, 2, 3, 4 = SAFETY RODS IN MOVABLE HALF
5, 6, 7, 8 = SAFETY RODS IN FIXED HALF

A, *B* = CONTROL RODS IN MOVABLE HALF
C, *D* = CONTROL RODS IN FIXED HALF
S = SERVO CONTROL IN MOVABLE HALF

FUEL ELEMENT DETAIL

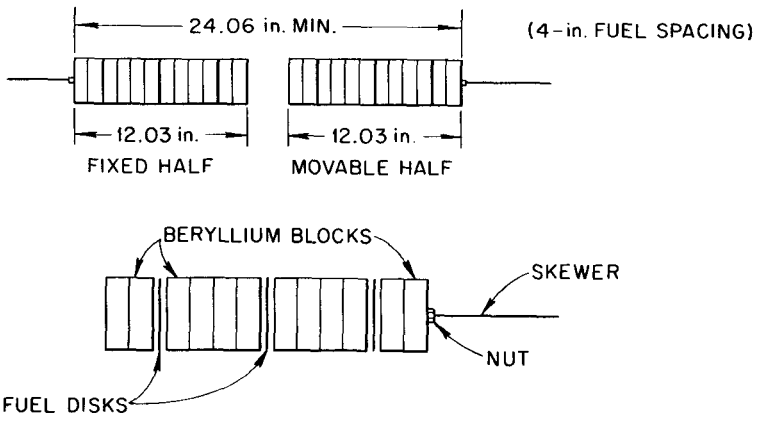

Fig. 3. Arrangement of Core Elements in CA-18 (Fixed Half Interface)

Table 1. Comparative Descriptions of CA-1 and CA-18

	CA-1	CA-18
Outside Dimensions	21.0 x 21.0 x 23.3 in.	24.0 x 28.4 x 24.1 in.
Spacing of 10-mil-thick fuel disks	1 in.	4 in.
Volume fractions:		
Aluminum (grid and skewers)	0.0610	0.0611
Beryllium (moderator)	0.9060	0.9128
Uranium (fuel)	0.0064	0.0016
Stainless steel (skewers)	0.0004	0.0003
Void	0.0262	0.0242
U^{235} loading	18.08 kg	7.65 kg
k_{eff}	1.0054	1.0020
Be:U^{235} atomic ratio	390	1560

skewers plus an artificial quantity having the same absorption cross section as the impurities in other parts of the system. Table 1 and Figs. 2 and 3 describe the nearest approaches to simple unreflected cubical critical assemblies for each of the two fuel spacings. In subsequent experiments the necessary excess multiplication was provided by placing additional core elements just outside of the clean assembly.

II. EXPERIMENTAL MEASUREMENTS

Measurements with CA-1

Initial Approach to Criticality. In the approach to criticality with CA-1 (see Fig. 2) uranium fuel disks were added to the core elements nearest the center of a 24 x 24 x 25 in. beryllium-reflected array until the assembly became critical. Except for one missing corner fuel element, this first array consisted of a 4 x 4 cell core with a 6-in.-thick reflector on four sides. It contained 6.05 kg of U^{235}. At criticality one control rod in the reflector (rod D in cell M-10) was withdrawn 3.7 in. The unreflected critical assembly was reached by alternately removing outside beryllium and adding fuel. The final unreflected parallelepiped had the dimensions 21.0 x 21.0 x 23.22 in., each of the 49 elements consisting of a 23-in. total thickness of beryllium and 22 fuel disks of average thickness 0.01 in. The assembly contained 18.08 kg of U^{235} and was critical with control rod C withdrawn 2.59 in., corresponding to 0.0054 in reactivity.

The experimental critical mass of the unreflected assembly was approximately 27% below that predicted in the multigroup calculations.[8] Since this disagreement was larger than expected, the experimental work described below was performed in an effort to locate any possible experimental errors of this magnitude.

Control Rod Calibration. In a control rod calibration, rod C was found to have a total value of \$2.82 by comparison with rod-drop measurements of the symmetrically located safety rods 7 and 8. The calibration curve shown in Fig. 4 was constructed by assuming a form similar to the detailed calibration measured in CA-18 and normalizing to a total value of \$2.82. This curve was used for subsequent reactivity comparisons. No detailed control rod calibration measurements were made on CA-1.

Reactivity Measurements. The experiments intended to determine the effect on the reactivity of spurious reflections from surrounding materials are summarized in Table 2. Reactivity values were found by comparing known control rod positions with the calibration of Fig. 4. In the first experiment listed, the neutron trap below the assembly was designed to cut off any reflected neutrons from the floor and structure; however, the reflected neutrons from the trap were found to be more effective than those from the floor. In one experiment (No. 7) the entire parallelepiped was moved up 27 in. to the

8. A. O. Mooneyham, NEPA-1710, op. cit.

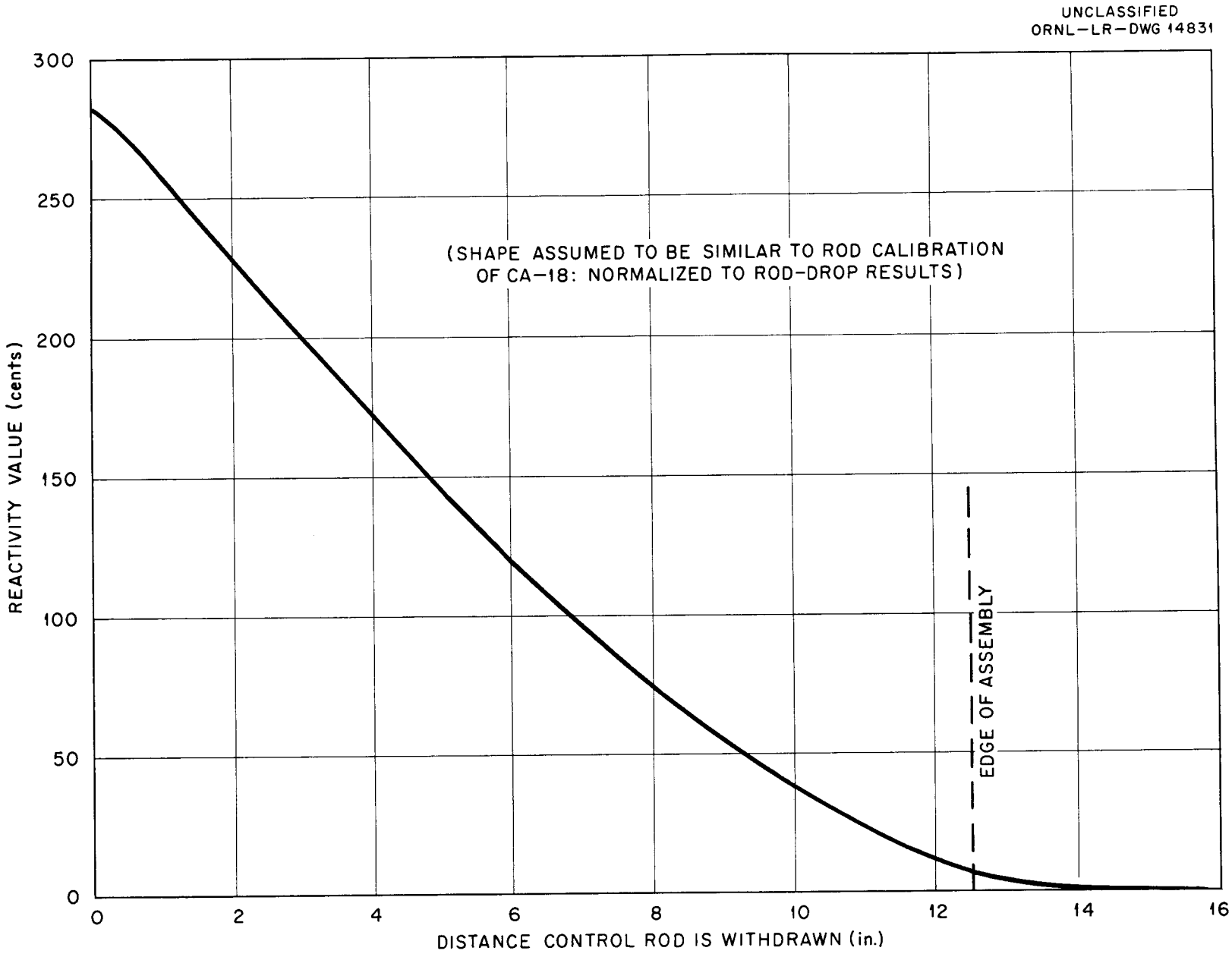

Fig. 4. Calibration of Control Rod C in CA-1.

Table 2. Effect of Various Surrounding Materials on the Reactivity of CA-1

Experiment Number	Description of Material[a]	Gain in Reactivity Over Basic Assembly (¢)
1	36 x 45 in. neutron trap was added below assembly; trap consisted of 8 in. of air space, 0.017 in. of cadmium, 1 in. of plexiglas, and 3 in. of graphite[b]	31.5
2	Same as No. 1 except a 1/4-in.-thick by 36 in. boral sheet was added 2-1/2 in. below the assembly (i.e., between the assembly and the cadmium)	19.8
3	Same as No. 2 except all plexiglas and graphite was removed	3.5
4	1/4-in.-thick boral sheet was placed on four sides of assembly (no air spaces)	73.5
5	1-in.-thick boral sheet was placed 2 in. from bottom of assembly (i.e., a 2-in.-thick air gap existed between the assembly and the boral)	37.3
6	Layer of pressure tape covered one side of assembly (similar tape was used to cover the boral plates used in the above measurements)	4.5
7	Entire critical assembly was raised 27 in. to uppermost position in the aluminum grid	69.0
8	Two pieces of 3 in. by 1-3/8 in. steel channel[c] were added to the top of the assembly; the assembly remained in the uppermost position in the grid	88.6
9	Assembly was returned to the center of the grid, and a 1-in.-thick aluminum sheet was added to the top and one side of the assembly	126.9
10	One of the 1-in.-thick aluminum sheets used in No. 9 was moved out, leaving a 3-in.-thick air gap between the assembly and the aluminum	26.8

a. The aluminum grid was supported on a 3/4-in.-thick steel table top, 26 in. above the floor.
b. Listed in order of placement from bottom of assembly.
c. Four similar channels were part of the normal structure.
d. The average total thickness of aluminum in the grid outside of the assembly was 1.57 in.

uppermost position in the grid. Again a gain in reactivity resulted, this time caused by an increase in the number of neutrons reflected from the structural steel used to hold the aluminum grid in place. Experiments 9 and 10 were performed in order to exaggerate the effects of the external aluminum grid and thereby set an upper limit on this contribution.

Some inconsistencies in the control rod positions for criticality were observed in the above measurements. All movable parts of the system were found to be mechanically reproducible, and the reason for the inconsistencies had not been ascertained at the time the assembly was dismantled. The difficulty was later attributed to photoneutrons from the beryllium, but no quantitative conclusions could be drawn.

Miscellaneous Measurements. One measurement of the uranium cadmium fraction (CF)* was made by comparing the activation of the fuel disk nearest the geometric center of the assembly to that of a similar fuel disk covered with 0.02 in. of cadmium. This gave a cadmium fraction value of 0.46. The accuracy of this measurement is questionable owing to uncertainties in the fuel disk background as well as in the counting correction factors.

Power distributions within the assembly were observed by measuring the gamma-ray activity of fuel disks. The results were in substantial agreement with the expected cosine distribution as indicated in Figs. 5 and 6. The terms lateral and longitudinal are used to define directions parallel or normal, respectively, to the interface of the two assembly halves.

A danger coefficient measurement on the fuel was made by removing the fuel disk nearest the center of the assembly and replacing it with a smaller fuel disk. The observed loss in specific reactivity was 2.9¢/g of U^{235}. Assuming the fuel importance to be proportional to the flux squared and assuming the value 100¢ to be equivalent to 0.0073 of the reactivity, it was found that $\delta k/k = 0.475\, \delta M/M$, where M is the mass of U^{235} in the critical assembly.

Measurements with CA-18

Initial Approach to Criticality. The first critical array of CA-18 (Fig. 2) had an over-all size of 27 x 27 x 24 in. Except for the four missing corner fuel elements, the array consisted of a 7 x 7 cell core with a 3-in.-thick beryllium reflector on four sides. It contained 4.97 kg of U^{235} and was critical with one control rod in the reflector (rod D) displaced 2.25 in. The final unreflected critical assembly had dimensions 24.00 x 28.40 x 24.06 in. and contained 7.65 kg of U^{235}. This unreflected assembly was critical with control rod A in the core displaced 2.60 in., corresponding to 0.0020 in reactivity.

Control Rod Calibration. An absolute calibration, that is, one that is independent of delayed neutrons or transients, was made for CA-18. This was done by observing the displacement of control rod A caused by the addition of

* $CF = (N_b - N_{Cd})/N_b$, where N_b is the activation of the bare disk and N_{Cd} is the activation of the disk having a 20-mil-thick cadmium cover on each side.

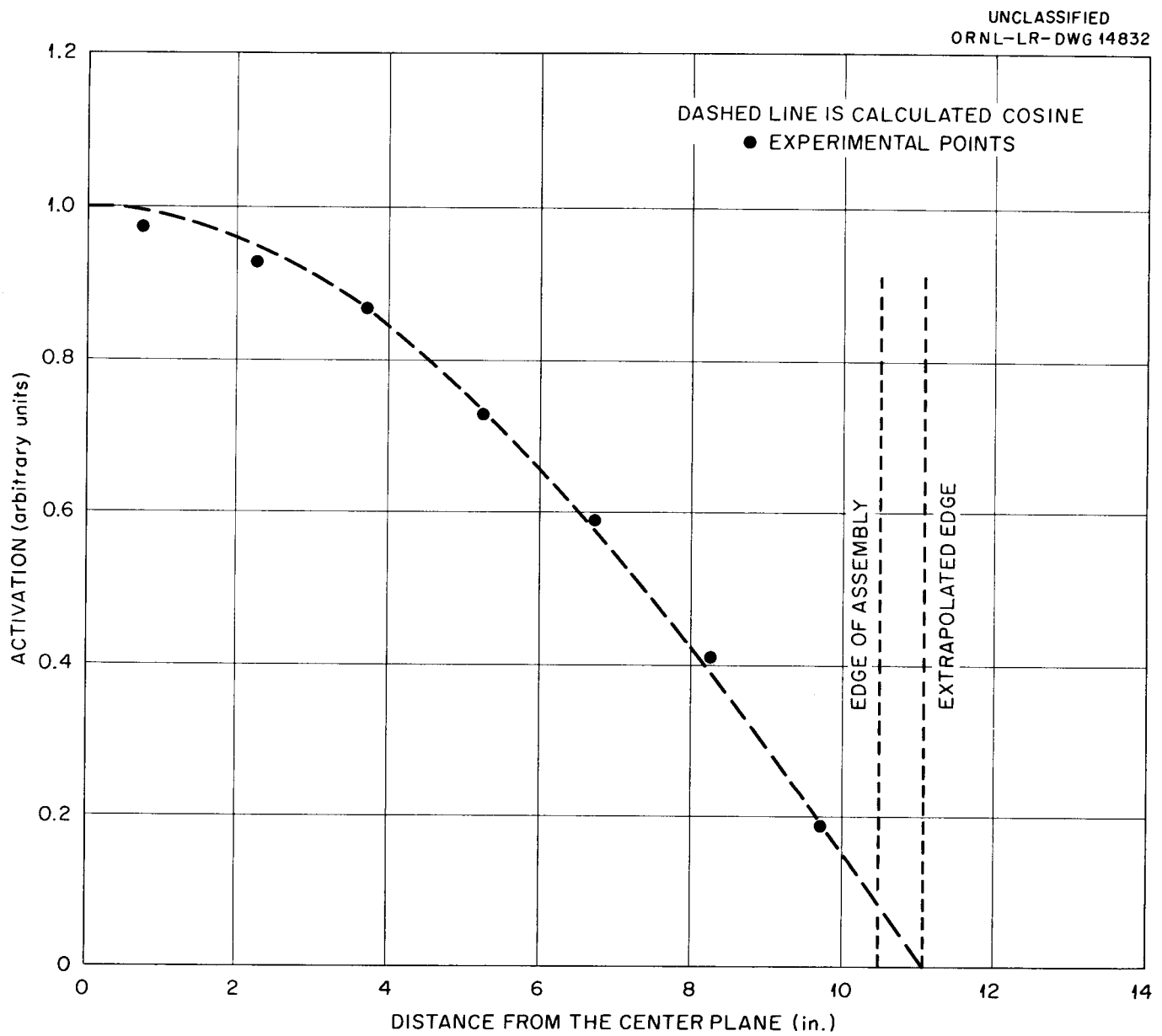

Fig. 5. Power Distribution Along a Lateral Axis in CA-1 (Gamma-Ray Activity of Uranium Disks).

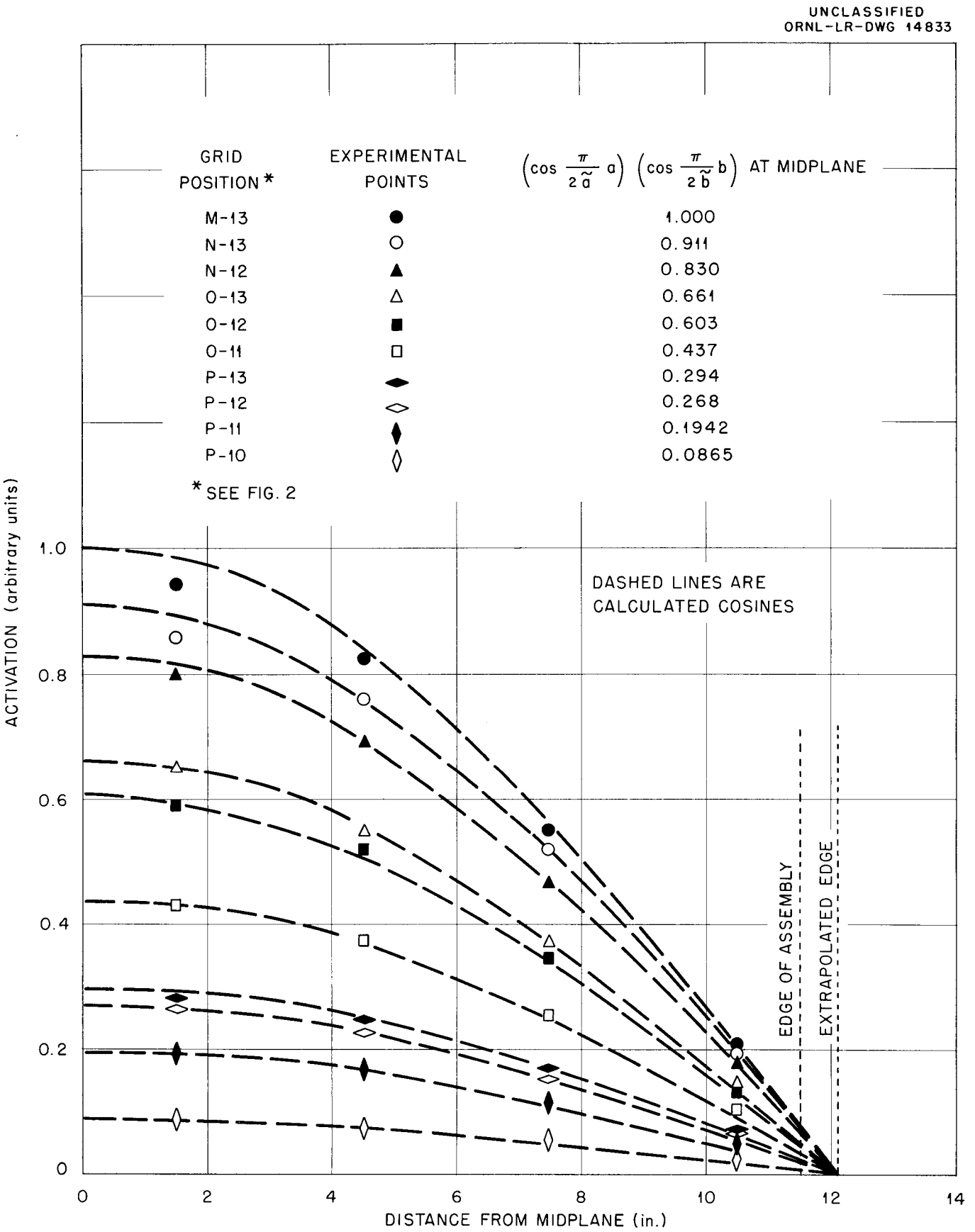

Fig. 6. Power Distribution Along Several Longitudinal Traverses in CA-1 (Gamma-Ray Activity of Uranium Disks).

a 1/4-in.-thick layer of beryllium on top of the assembly and assigning to the displaced portion of the rod the same reactivity value as that calculated for a change in the buckling of the system caused by the addition of the beryllium. The calculation, which is presented in Appendix A, is probably accurate within 2%. Control rods B, C, and D were then calibrated against control rod A.

The control rod sensitivity, i.e., the change in reactivity per inch of travel, is shown in Fig. 7 for each of the rods in CA-18. The control rod position is the displacement from the center of the assembly, or the distance the rod is withdrawn. The maxima particularly prominent in the sensitivity curve for rod A occur when the fuel planes in the rod are misaligned with those in the stationary part of the assembly. The steep part of the curve in the vicinity of the edge of the assembly is due to the effect of "plugging" the control rod channel. This effect may be otherwise thought of as due to adding moderator in its region of highest importance. The control rod calibration curves in Fig. 8 were found by integrating the sensitivity curves from infinity to any particular position.

Conventional rod drop and pile period observations were also made for comparison with the absolute calibration of the rods; however, these calibration methods depend on a knowledge of the effectiveness of delayed neutrons and are complicated by the presence of photoneutrons from beryllium. Pile period observations are particularly difficult owing to a number of photoneutron groups arising from long-lived fission-fragment hard gamma-ray emitters. Table 3 is a comparison between the reactivity values determined from the pile period observations and those obtained in the absolute calibrations. Reactivity values from the pile period observations were calculated from five delayed neutron groups[9] through use of the in-hour equation, neglecting delayed photoneutrons from the beryllium. The inconsistency of the ratio of the results from the two methods reflects the inherent uncertainty in the effective value of delayed neutrons, and the effect of the delayed photoneutrons from the beryllium. Further, the apparent period is strongly influenced by the operational history of the system.

In Table 4 the control rod reactivity values obtained by the rod drop method, using a total delayed neutron fraction of 0.0073, are compared with the total control rod reactivity values obtained by the absolute calibration method (see Fig. 8). Again, the lack of consistency is no worse than expected in view of the experimental uncertainties in the two methods.

Both the pile period and the rod drop results are about 80% of the corresponding absolute reactivity value. Apparently the best values found by the pile period method are those from the shorter period range.

Foil Exposures. Several types of foil exposures were made within CA-18. Indium-aluminum foils were used to obtain indium activation measurements. In addition, fission rates within the assembly were determined by observing the activity of fission fragments on thin aluminum "catcher" foils which were in direct contact with fuel disks during an exposure. The activities of similar

9. S. Glasstone and M. C. Edlund, "The Elements of Nuclear Reactor Theory," p. 65, D. Van Nostrand Company, Inc., 1952.

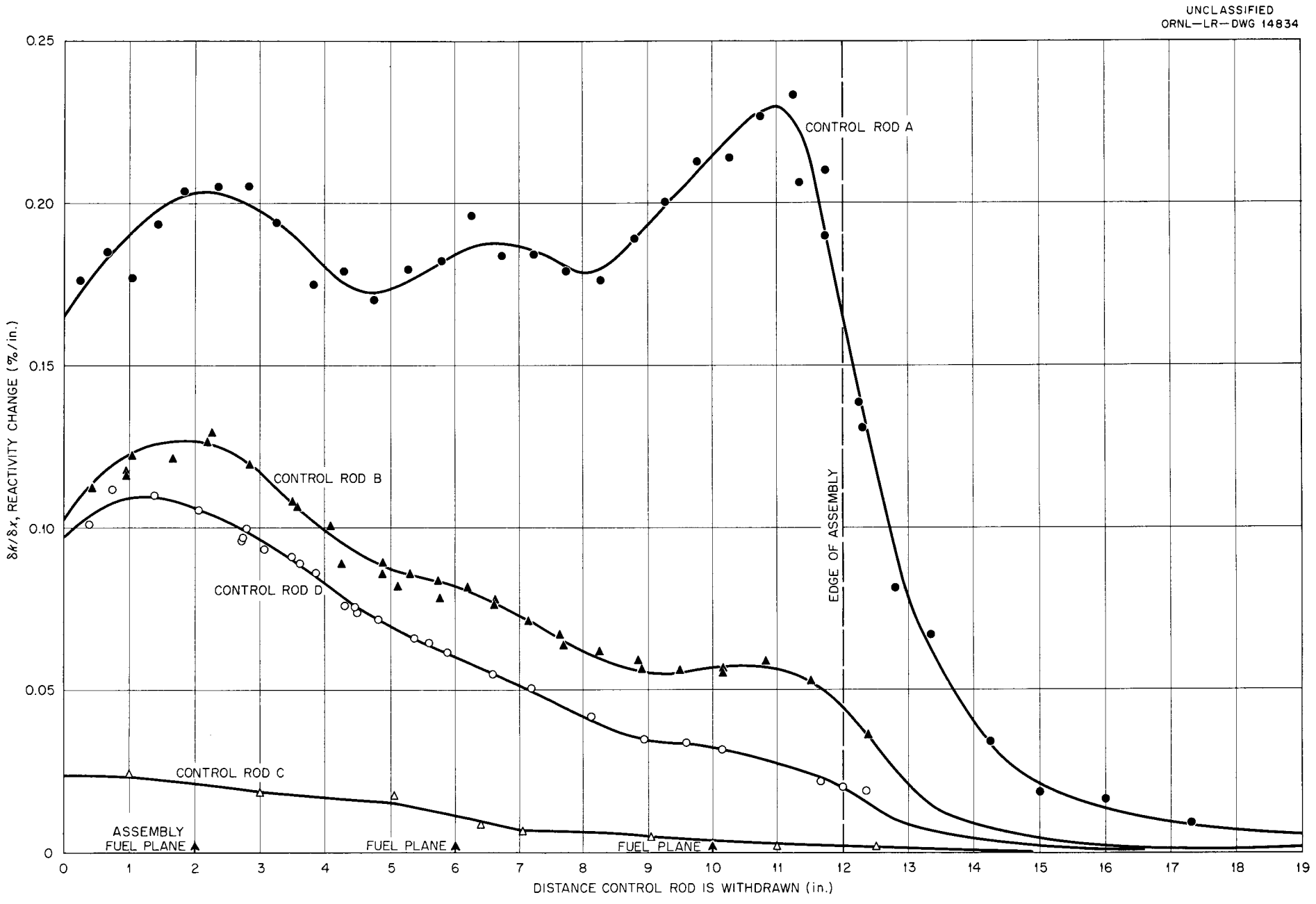

Fig. 7. Change in Reactivity of CA–18 as a Function of Withdrawal of Control Rods.

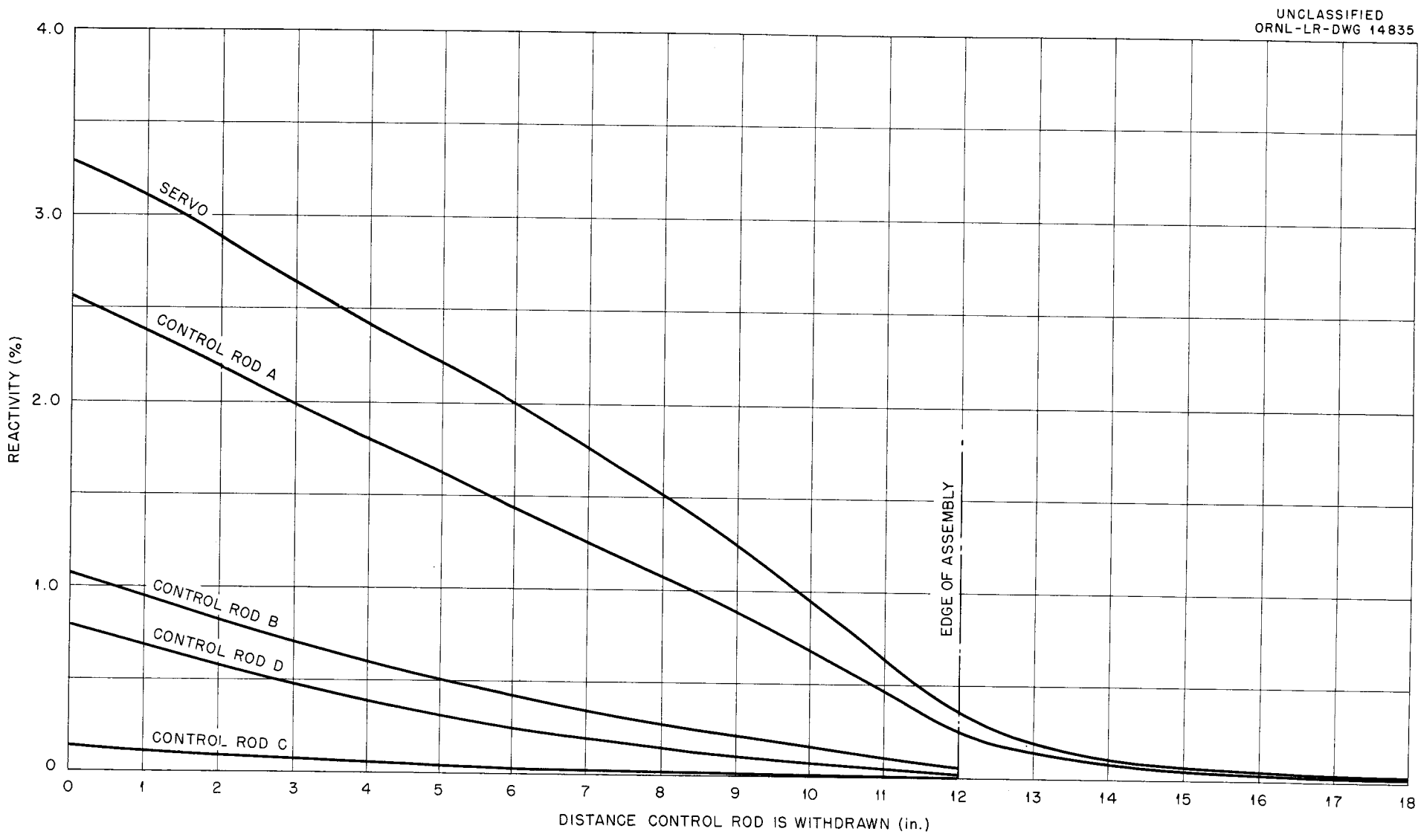

Fig. 8. Calibration Curves for Control Rods in CA-18.

Table 3. Comparison of Reactivity Values of Control Rods in CA-18 Determined by Pile Period and by Absolute Calibration Methods

Observation	Period (sec)	Reactivity: Pile Period Method	Reactivity: Absolute Method	Ratio of Reactivities, Pile Period:Absolute
1	770.0	0.000117	0.000182	0.646
2	521.0	0.000170	0.000460	0.369
3	417.0	0.000209	0.000347	0.603
4	166.6	0.000471	0.000610	0.773
5	152.0	0.000507	0.000588	0.863
6	101.3	0.000697	0.000873	0.799
7	95.6	0.000733	0.000920	0.798
8	95.6	0.000733	0.00111	0.661
9	84.8	0.000795	0.000940	0.846

Table 4. Comparison of Reactivity Values of Control Rods in CA-18 Determined by Rod Drop[a] and Absolute Calibration Methods

Safety Rod	Equivalent Control Rod	N_o	N_i	Reactivity: Rod Drop Method	Reactivity: Absolute Method	Ratio of Reactivities, Rod Drop:Absolute
1	C	39.0	35.0	0.000831	0.00143	0.581
3	D	34.8	19.1	0.00600	0.00793	0.757
6	B	38.0	18.0	0.00810	0.01070	0.757
5	A	37.5	9.1	0.02385	0.02564	0.928

a. In the rod drop method, $\delta k/k = 0.0073\ (N_o - N_i)/N_i$, where N_o is the initial power level and N_i is the power level extrapolated to the time immediately following the rod drop; see, for example, Ref. 9, p. 305, Eq. 10.35.3.

catcher foils which were exposed within a composite fuel disk, that is, a disk consisting of five individual disks, were used to study the effect of the self shielding of the fuel.

The indium-aluminum foils were each 5/16 in. in diameter and 10 mils thick, having an effective indium thickness of 0.3 mil or 5.4 mg/cm^2. For one exposure the foils were placed along a horizontal lateral line (that is, parallel to the fuel plane) which was 1/4 in. from the midplane. Plots of the relative activity of the foils for this traverse are shown in Fig. 9 and are in substantial agreement with the expected cosine distribution. Similar measurements (Fig. 10) along the longitudinal axis of the assembly (that is, perpendicular to the fuel plane) indicate sharp depressions in the flux near the fuel planes, but the plots are enveloped by cosine curves. The indium-cadmium fraction - - obtained by comparing the activity of bare foils to that of foils covered with 20-mil-thick cadmium covers - - varies from a maximum of 0.4 between the fuel planes to a minimum of 0.3 at the fuel planes.

Fission rates determined by the catcher foil technique are shown in Figs. 11 and 12 for foil exposures along the lateral and longitudinal axes, respectively. In some cases measurements on opposite sides of the same fuel disks are indicated. The cadmium fraction for fuel is seen to vary between 0.852 and 0.880. (The cadmium covers used in these measurements were also 20 mils thick.)

The variation of the fission rate within the composite fuel disk consisting of five 2-mil-thick disks is shown in Fig. 13. This composite disk replaced one of the conventional 10-mil-thick disks during the measurements. The average fission rate throughout the 10 mils was found to be 89.2% of the average surface fission rate on the disk.

Reactivity Measurements. A number of experiments were performed to determine the effect on the reactivity of CA-18 of introducing various materials into the assembly. In the first group of experiments, the core element in cell K-13 (see Fig. 3), the cell nearest the center of the assembly, was pushed back from the midplane so that a sample of material could be placed very near the center of the assembly. The changes in reactivity caused by various materials in this position are summarized in Table 5. All of the samples were 2-7/8 in. square having the thicknesses indicated in Table 5. The reactivity values listed are found from the changes in control rod positions necessary to compensate for the addition of the sample into this space, that is, the difference in the reactivity of the assembly with the sample in place and the reactivity of the assembly with an air space of equal thickness at the same location.

The effects on the reactivity of other materials were observed in a similar way in cell L-15. The results of these tests are listed in Table 6. The liquid samples were contained in a thin-walled stainless steel can, 1 x 2-7/8 x 2-7/8 in., and their reactivity values were corrected for the effect of the can. Furfural, $H_4C_5O_2$, is an organic material having a hydrogen density approximately one-half that of water. The sample labeled "1/2 Plexiglas" was prepared by drilling small holes in a Plexiglas block to reduce its mass from 157.7 g to

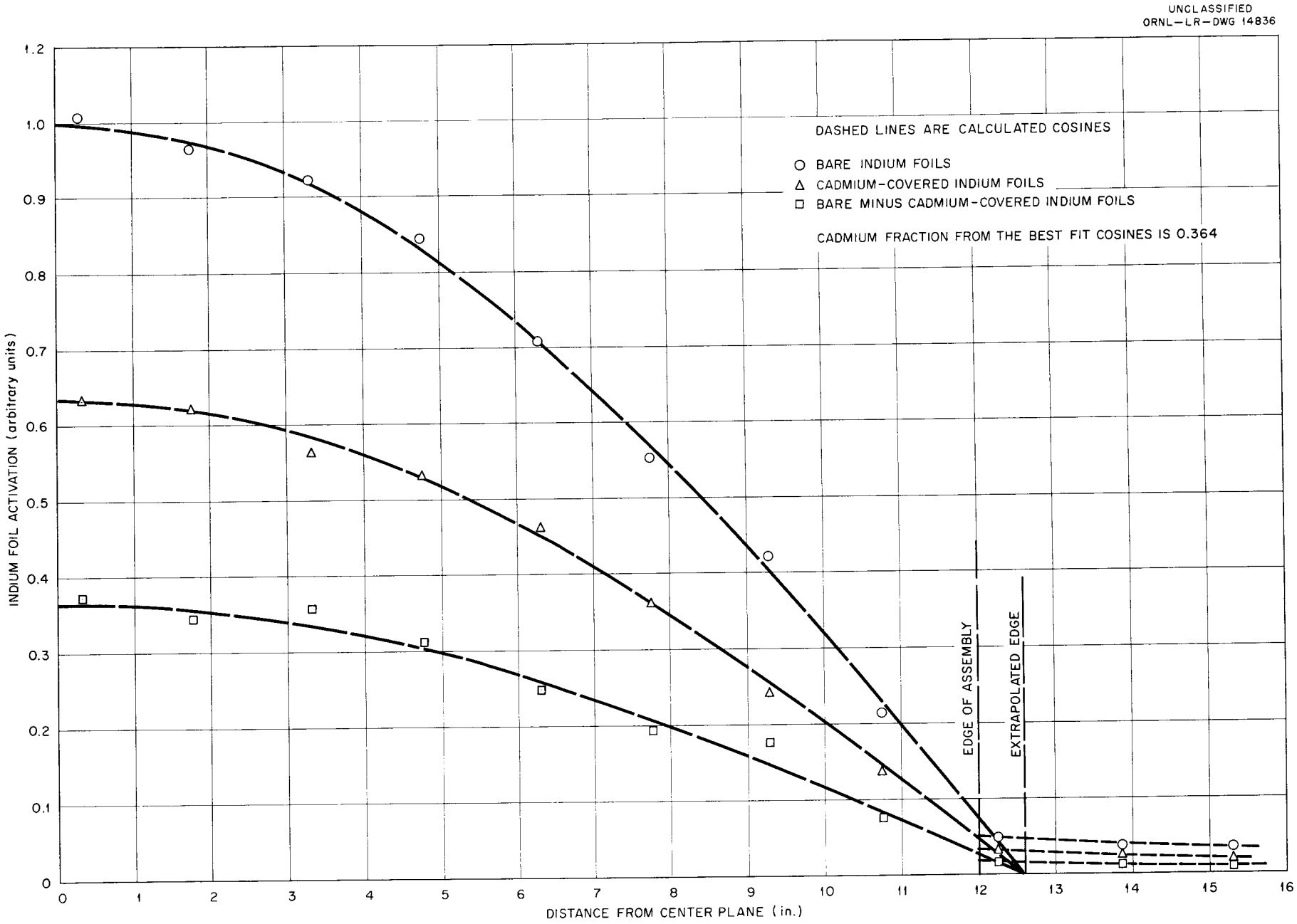

Fig. 9. Activation of Indium Foils Along a Horizontal Lateral Traverse (¼ in. from Midplane) in CA-18.

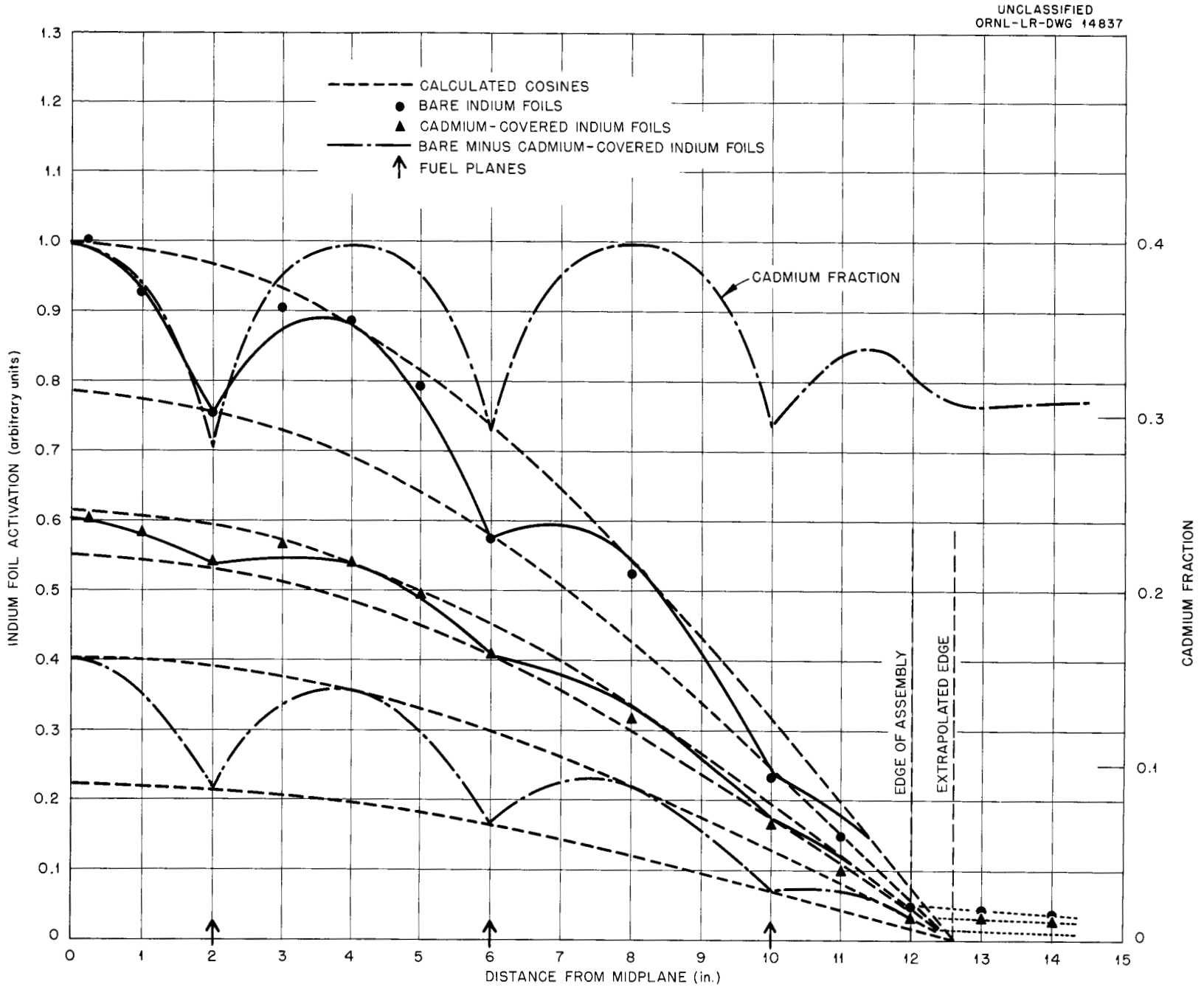

Fig. 10. Activation of Indium Foils Along the Longitudinal Axis of CA-18.

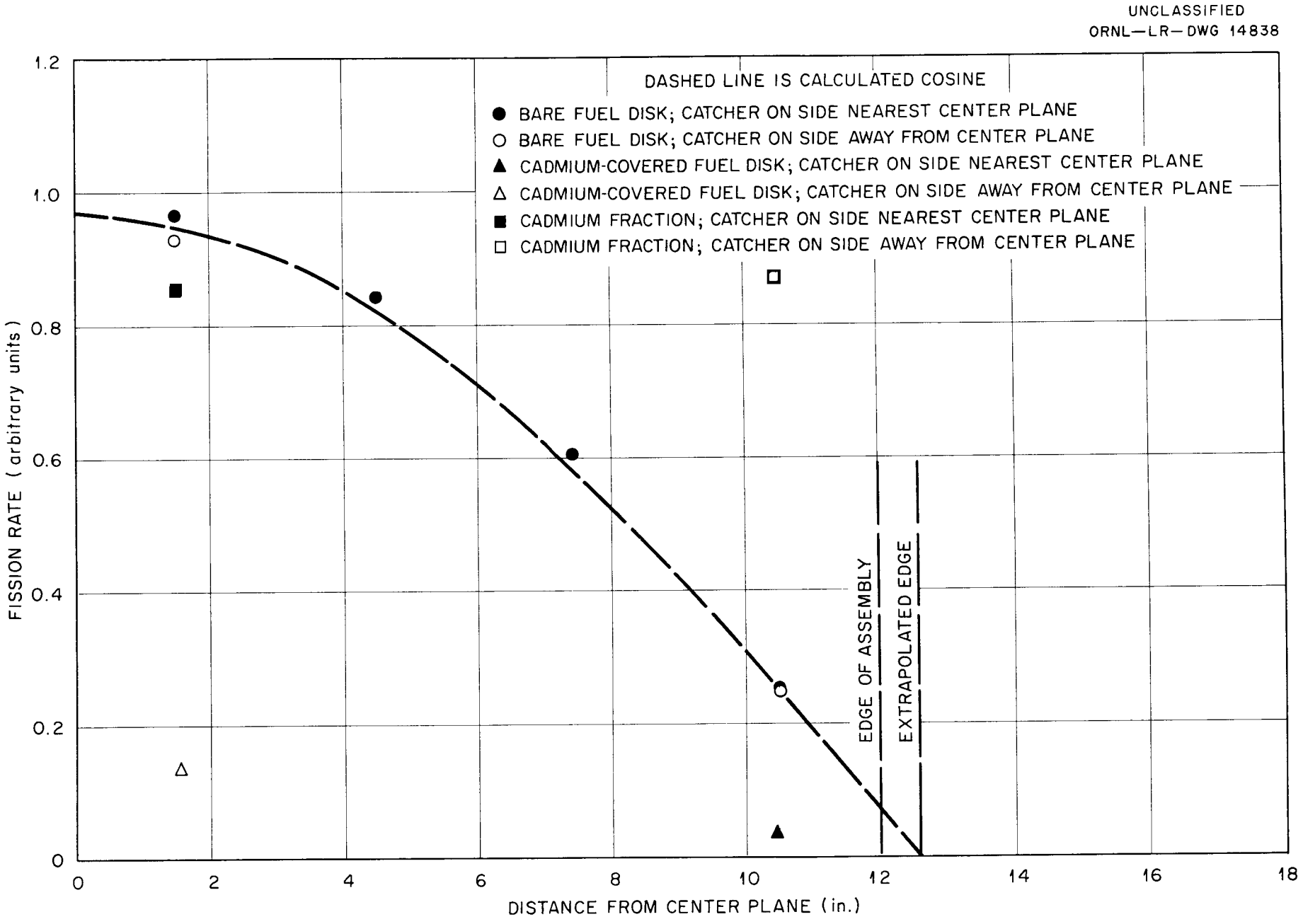

Fig. 11. Power Distribution Along a Lateral Axis of CA–18 (Fission Rate of Fuel Disks).

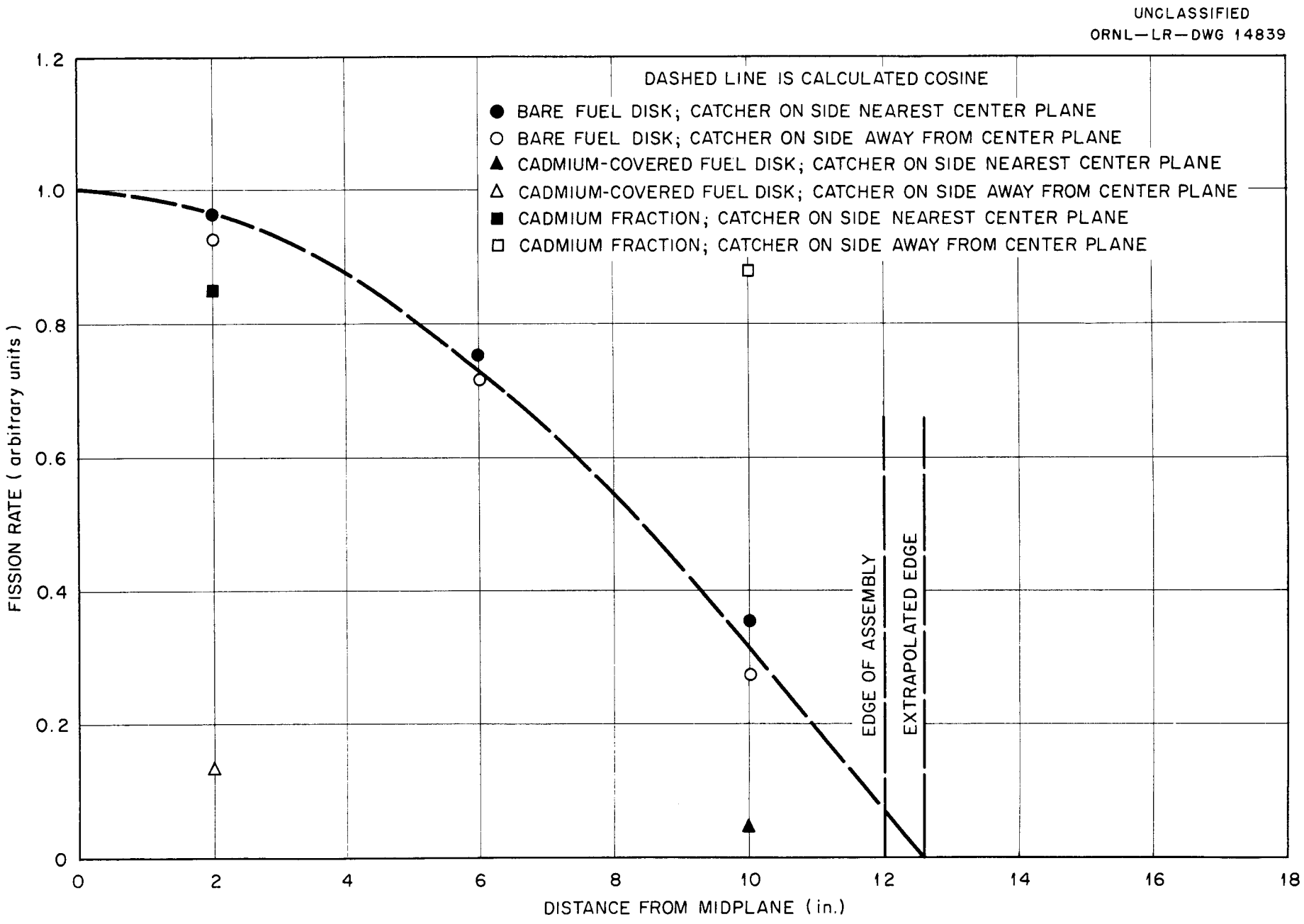

Fig.12. Power Distribution Along the Longitudinal Axis of CA–18 (Fission Rate of Fuel Disks).

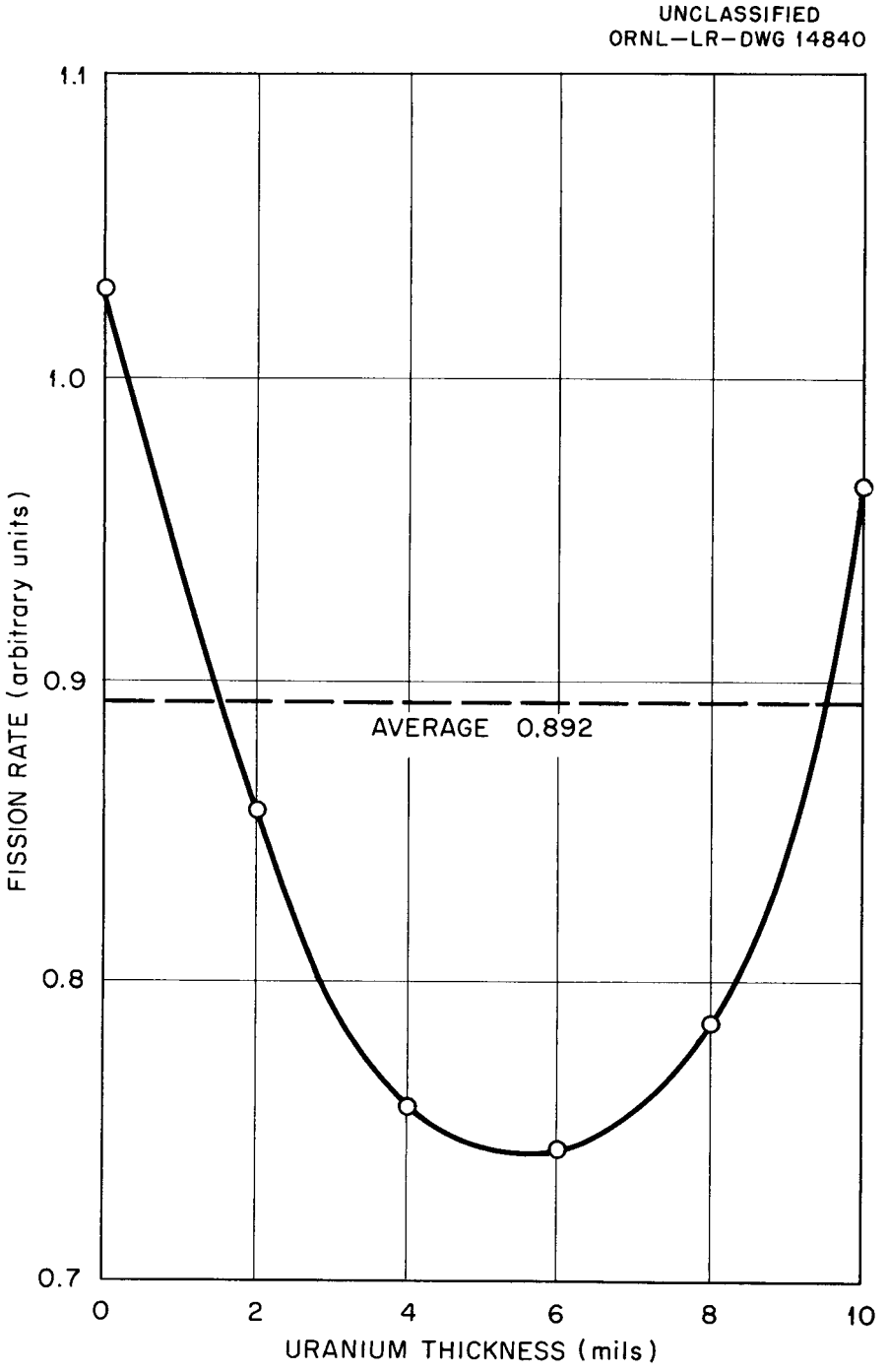

Fig. 13. Self-Shielding Factor for a 10-mil-Thick Fuel Disk in CA-18.

Table 5. Reactivity Values of Various Materials Inserted in Cell K-13 Near the Center of CA-18

Sample	Thickness (in.)	Mass (g)	Atomic Weight (g/mole)	Number of Moles	Reactivity,[a] $\delta k \pm 0.00002$	δk/mole ($\times 10^{-3}$)
Mg	0.500	115.78	24.32	4.760	+0.00024	+0.0504
Fe	0.500	523.68	55.85	9.376	-0.00902	-0.963
Ti	0.320	185.67	47.90	3.876	-0.00936	-2.42
Al	0.500	179.3	26.97	6.648	-0.00864	-1.301
Ni	0.160	183.15	58.69	3.121	-0.00584	-1.870
Mo	0.425	475.2	95.95	4.953	-0.01050	-2.120
Cb	0.250	277.42	92.91	2.986	-0.00335	-1.121
Teflon	0.500	152.28	-	-	+0.00001	-

a. Compared to reactivity of assembly with a void of equal volume.

Table 6. Reactivity Values of Various Materials Inserted in Cell L-15 Near the Center of CA-18

Sample	Thickness (in.)	Mass (g)	Reactivity,[a] $\delta k \pm 0.00005$
Furfural[b]	1.0	150.1	-0.00005
Water[b]	1.0	127.6	-0.00009
1/2 Plexiglas	1.0	83.5	+0.000003
Graphite	7.25	1624.3	+0.00010
Teflon	7.25	2026.02	-0.00005

a. Compared to reactivity of assembly with a void of equal volume; values for Furfural and water samples were corrected for stainless steel containers.
b. Contained in thin-walled stainless steel can.

83.5 g. Teflon $(CF_2)_n$ is of interest as a common material used in other zero power critical assemblies. Since cell L-15 is off center, absorption and scattering effects of the samples somewhat cancel each other. No significant differences between water, Furfural, 1/2 Plexiglas, and Teflon are apparent, although the large graphite block was observed to be significantly better as a scatterer than the Teflon block of the same size.

The effect of the fuel heterogeneity in the assembly was determined by observing the increase in the reactivity caused by replacing the 10-mil-thick disks in one-half of the element in cell L-14 with uniformly spaced 2-mil-thick disks having the same total mass. In another test the number of 2-mil-thick disks used was reduced such that the total reactivity value of the element was approximately the same as that of a normal element. The results of these observations are presented in Table 7. For purposes of comparison, the reactivity values of cell M-13 with a normal fuel loading and without any fuel are also given. Cell L-14 is nearer the center of the assembly than cell M-13, which explains the higher reactivity values. The results given in Table 7 are only a qualitative indication of self shielding. Since the neighboring fuel elements were not changed, the effectiveness of the thin disks in positions intermediate to the normal fuel positions was exaggerated.

Table 7. Reactivity Value of Fuel in CA-18

	Half-Cell Description			Reactivity Value		
Cell No.	Number of Fuel Disks	Thickness of Each Disk (mils)	Total U^{235} Mass (g)	Of Total Half-Cell	Of U^{235} in Half-Cell	Of 1 g of U^{235} in Half-Cell
L-14	0	-	0.0	0.02307[a]	-	-
L-14	3[b]	10	50.3	0.02890	0.00583	0.000116
L-14	15	2	50.3	0.03222	0.00915	0.000182
L-14	8	2	26.8	0.02873	0.00566	0.000211
M-13	0	-	0.0	0.02204[a]	-	-
M-13	3[b]	10	50.3	0.02760	0.00556	0.0001105

a. Represents reactivity value of all materials in half-cell except fuel.

b. Normal loading for half-cell.

III. MULTIGROUP CALCULATIONS

Several reactor multigroup calculations were performed and the resulting values of the effective multiplication of CA-1 and CA-18 were compared to the experimental values. The method of calculation and the notation were basically the same as those reported earlier.[10] In order to show the approximations used, the derivation of the criticality equation is repeated in Appendix B.

Eight variations of the basic calculations were used to compare the effects of various corrections. In the paragraphs below the assumptions common to all the calculations are discussed first. These are followed by descriptions of the variations in the calculations, a summary of which is given in Table 8. The results of the calculations are then presented and comparisons are made.

General Calculation Procedure. The calculations were made using 32 energy groups from 10^7 ev to thermal. The cross-section data were taken from published curves[11] and logarithmic averages were found for each energy group. The cross-section values and the fission source distribution are given in Appendix C.

The uranium macroscopic cross sections in each group were reduced to values corresponding to an equivalent homogeneous system. As discussed below, corrections were made in some of the calculations to account for fuel lumping and the associated self-shielding effect.

The scattering of neutrons in the uranium was considered to be isotropic for all energy groups. Except in the special cases specified below, the scattering in the beryllium was also assumed to be isotropic.

The effective leakage cross section, DB^2, for each group includes the variation of λ_{tr} with energy since $D = 1/3\ \lambda_{tr}$ and B^2 is a function of the extrapolation distance, $0.71\ \lambda_{tr}$.

Variations in Calculations

Uranium Self-Shielding Corrections. With the exception of Method I, one of two different corrections[12] was made in each calculation to compensate for the lumping of the fuel in the experimental assemblies. One of the corrections, called the P_0 correction, was calculated under the assumption that the neutrons entered the absorber isotropically. The second, i.e., the P_1 correction, allowed for some directional preference or a flux depression outside of the uranium. Methods of calculating both corrections are given in Appendix D. The self-shielding factors resulting from these calculations are compared in Fig. 14.

---

10. C. B. Mills, ORNL-1493, op. cit. pp5, 115-117.
11. Publications by the Neutron Cross Section Advisory Group, AECU-2040, BNL-170, BNL-170A, BNL-170B.
12. J. C. Bartels, "Self-Absorption of Monoenergetic Neutrons," KAPL-336 (1950).

Table 8. Description of the Various Calculations

Method Number	Code Description
I	A, B-1, C-1, D-1, E-1, F-1, G-1
II	A, B-2, C-1, D-1, E-1, F-1, G-1
IIa	A, B-2, C-2, D-1, E-1, F-1, G-1
III	A, B-2, C-1, D-2, E-1, F-1, G-1
IV	A, B-3, C-1, D-2, E-1, F-1, G-1
V	A, B-3, C-1, D-2, E-1, F-1, G-2
VI	A, B-3, C-1, D-2, E-2, F-1, G-1
VII	A, B-3, C-1, D-2, E-1, F-2, G-1

Code Definitions:

A. Multigroup calculation using general calculation procedure described on page 25 and in reference 6.

B-1. No correction made for uranium self shielding.
B-2. P_0 " " " " " " .
B-3. P_1 " " " " " " .

C-1. Elastic scattering in U^{235} for all energies.
C-2. Inelastic " " " " energies >1 Mev.

D-1. Isotropic scattering in Be for all energies.
D-2. Anisotropic " " " " energies >1 Mev.

E-1. Elastic scattering in Be for all energies.
E-2. Inelastic " " " " energies >1 Mev.

F-1. Neutron slowing-down density of $\phi \xi \Sigma_t$.
F-2. " " " " " $\phi \xi \Sigma_s$ (Fermi model).

G-1. No correction for effect of external aluminum grid.
G-2. Correction for effect of external aluminum grid.

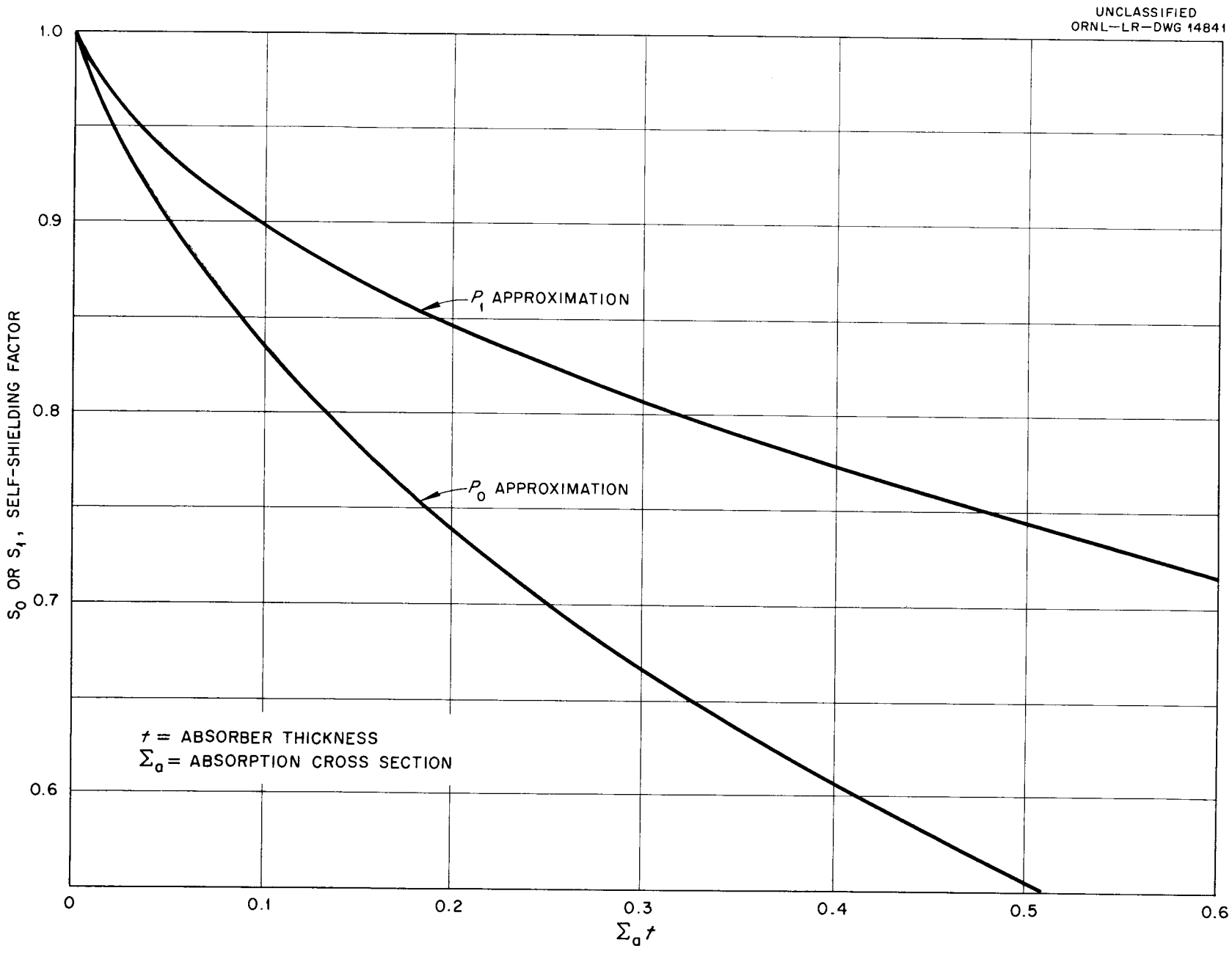

Fig. 14. Uranium Self-Shielding Factors Calculated by P_0 and P_1 Approximations.

Elastic Versus Inelastic Scattering in U^{235}. In general, the neutron scattering in uranium was assumed to be elastic. However, an inelastic scattering correction was included in the IIa calculation of CA-1. Since the effect was small, a similar calculation was not made for CA-18 in which the average neutron energy was lower.

Isotropic Versus Anisotropic Scattering in Beryllium. In methods I, II, and IIa, the neutron scattering in beryllium was considered to be entirely isotropic. In methods III through VII corrections were made for anisotropic scattering of neutrons with energies higher than 1 Mev. These corrections affected the multigroup calculation through variations in the transport cross section, σ_{tr}, and the lethargy gain per collision, ξ, values of both having been determined from differential scattering data[13] which were corrected to the center-of-mass system. Estimates were also made of the number of neutrons scattered to energies below the threshold of the U^{238} fission detector used in the differential scattering experiment and the data were corrected accordingly. These corrected data could not be well approximated by the simple addition of a p-scattering term, although it was possible to evaluate $\bar{\mu}_o$, the average cosine of the scattering angle. Values of σ_{tr} and ξ were then calculated from $\bar{\mu}_o$.

Numerically integrating the corrected curve for differential scattering yielded the value

$$\bar{\mu}_o = \frac{\int_{-1}^{1} \mu\sigma(\mu)d\mu}{\int_{-1}^{1} \sigma(\mu)\, d\mu} = 0.254$$

for the average cosine of the scattering angle in the center-of-mass system with anisotropic scattering. Similarly, the value of $\bar{\nu}_o$, the average cosine of the scattering angle in the laboratory system with anisotropic scattering, was found to be 0.329. This is to be compared with a value of $\bar{\nu}_o = 0.074$ for the laboratory system with isotropic scattering.

The transport cross section σ_{tr} for the system with anisotropic scattering found by

$$\sigma_{tr} = (1-\bar{\nu}_o)\ \sigma_s$$

is thus smaller than its isotropic value by the factor

$$\frac{1-0.329}{1-0.074} = 0.725$$

13. E. T. Jurney, "Inelastic Collision and Transport Cross Sections for Some Light Elements," LA-1339 (Dec., 1951).

The calculation of the lethargy gain per collision, ξ, is presented in Appendix E and found to give a value of 0.150 for the system with anisotropic scattering. The corresponding value for the isotropic system is 0.206, the ratio of the two values being 0.728.

The product of the two ratios for σ_{tr} and ξ then is

$$(0.725)\ (0.728) = 0.527$$

and this was assumed to be the factor which should be used in the calculations to correct the product $\xi\,\sigma_{tr}$ to include anisotropic scattering in beryllium.

In order to test the validity of using this factor to include anisotropic scattering in the calculations, a calculation of the neutron age to thermal energy in beryllium was performed, the result of which could be compared with the accepted experimental value of τ. The relation used for this calculation of the age was

$$\tau = \sum_{i=1}^{th} \frac{\Delta u_i}{3\Sigma_s^i\ \xi_i\ \Sigma_{tr}^i}$$

where

Δu_i = lethargy width of energy group i,

Σ_s^i = macroscopic scattering cross section for energy group i,

ξ_i = lethargy gain per collision in group i as defined in the preceding paragraph,

Σ_{tr}^i = macroscopic transport cross section for energy group i.

When only isotropic scattering in beryllium was assumed, the value of τ calculated with this relation, using the fission source distribution and the cross section values from Appendix C, was 84.3 cm^2. The accepted experimental value is 98 cm^2. Anisotropic scattering was then included in the calculation in an attempt to approach the accepted value. This was done by multiplying the term $\xi\Sigma_{tr}$ in the upper energy range by the factor 0.527 determined in the preceding paragraph. The resulting calculated value of τ was 125 cm^2, which indicated a gross over-correction for anisotropic scattering.

This discrepancy in the age calculation is an obvious indication of either poor fundamental data or an inadequate calculation method. Approximately two-thirds of the value of the age is contributed by terms in the summation above 1 kev of neutron energy, so uncertainties in fission source distribution or cross sections in this range have an exaggerated effect.

If a correction factor of 0.762 instead of 0.527 had been used, the calculated value of τ would have been in agreement with the accepted value.

This higher value of the correction was the one actually used in Methods III through VII to account for anisotropic scattering in beryllium.

Nuclear Reactions in Beryllium. A number of nuclear reactions with beryllium, such as (n,2n), (α,n), (γ,n), and inelastic scattering, are known to take place. Experimental measurements of cross sections for any of these events are very difficult, and the results are questionable. An attempt to measure the cross section for the (n,2n) reaction resulted in an illogical range of values from 0.24 $\pm$ 0.07 barn, using a polonium-beryllium source, to -0.16 $\pm$ 0.13 barn, using a mock fission source;[14] therefore, no effort was made to consider this reaction in the present calculations. Neither are there any convenient methods for including the effects of the (α,n) and (γ,n) reactions; however, these effects are probably small.

A value of 0.38 barn for the inelastic scattering cross section for neutrons above 1 Mev has been reported,[13] which was found by subtracting the differential scattering cross sections integrated over a sphere from the total cross section. However, applying the corrections mentioned in the previous section to the observed data reduces the value of the cross section to 0.1 barn, which is so small that it may be completely obscured by experimental uncertainties. Nevertheless, it was included for one calculation of CA-1 (Method VI).

Methods of Computing Neutron Slowing-Down Density. With the exception of Method VII, the value of q, the neutron slowing-down density, was assumed to be equal to $q = \phi \xi \Sigma_t$. In Method VII the Fermi slowing-down form, $q = \phi \xi \Sigma_s$, was used. The scattering and total cross sections Σ_s and Σ_t included a leakage term DB^2.

Correction for Effect of External Aluminum Grid. An estimate of the effect of the external grid was made in Method V by calculating the return probability of leakage neutrons. The calculational procedure is given in detail in Appendix F. The distribution of first collisions of leakage neutrons in the external grid is calculated for a particular energy group i. Isotropic scattering in the grid is assumed and the probability of a scattered neutron being returned to the core is calculated. The convolution of first collision density and the return probability gives the total probability of a leakage neutron being returned. The returning neutrons are assumed to be distributed uniformly throughout the core such that their importance is 0.535 times that of a normal mode source distribution. The effective number of leakage neutrons of groups i which are returned to the core are added to the next lower, or i + 1, source term. This allows some slowing down due to the collision with aluminum and affords a convenient means of including the effect in the bare reactor multigroup procedure. Counting only first collisions gives a result for the number of scattering collisions which is too low. On the other hand, this assumption is somewhat self-compensating in that it allows the neutrons to return unattenuated from the scattering points. The assumption of isotropic scattering and the uniform distribution of the returning neutrons overestimate the effectiveness of the aluminum grid so that the result is an upper value.

---

14. H. M. Agnew, "Measurement of σ(n,2n) of Be^9," LA-1371 (Mar., 1952).

Results of the Multigroup Calculations.

The results of the various calculations described above are summarized in Table 9. Variations in the results caused by individual corrections are shown in Table 10. A qualitative picture representing the effect of some of the corrections may be seen in Figs. 15, 16, and 17 which are plots of the leakage, absorption, and fission distributions in CA-1.

The predominant variation in leakage (Fig. 15) occurs in the upper energy range and results from the inclusion of anisotropic scattering in beryllium. With anisotropic scattering the high-energy mean free paths are greater, resulting in an increased leakage in this region. As a result of increased high-energy leakage, fewer neutrons are available for the lower energy range. This is obvious from the absorption and fission distributions of Figs. 16 and 17.

Self-shielding corrections have the effect of shifting the spectrum toward the lower energy. With no self-shielding corrections, a greater fraction of neutron absorption will be indicated in the intermediate range, or just above thermal (around $u = 18$), and fewer neutrons will be available to the thermal group. On the other hand, self-shielding corrections cause relatively small changes in the total number of absorptions or fissions.

As was noted in Section II, each of the assemblies was critical with a control rod partially removed so that the clean assemblies described had values of k_{eff} slightly greater than one. The total variation in k_{eff} for all the cases reported in Table 10 is 14%. This is actually quite arbitrary and might easily be made to vary much more by means of a particular choice of data.

For example, the correction made for anisotropic scattering was adjusted to fit the thermal neutron age, but it is smaller than experimental observations of differential scattering would indicate. Using the correction 0.527, which was indicated by the experimental observations, instead of the adjusted value of 0.762, would change the value of k_{eff} as much as 20% from the isotropic case. On the other hand, the inclusion of the (n,2n) reaction might completely overbalance this negative correction. For example, an assumed cross section of 0.01 barn for the (n,2n) reaction above 0.3 Mev would introduce a change in k_{eff} around 4% in either CA-1 or CA-18. This assumed 0.01 barn may be compared to an experimental uncertainty as great as 0.10 barn.

Some of the multigroup results were used to calculate cadmium fractions for indium and uranium and neutron self-shielding factors in the fuel. These particular calculations are relatively insensitive to high-energy effects and show neutron energy distribution shifts, such as those caused by different self-shielding corrections. The calculated results are compared to experimentally determined quantities in Table 11. Experimental values for cadmium fractions vary widely due to the heterogeneity of the system as shown in Fig. 10. While no exact comparison can be made due to this variation, the calculated values for CA-18 are generally low, even for the P_0 self-shielding

Table 9. Summary of Results of Multigroup Calculations for CA-1 and CA-18: Comparison of Calculated k_{eff} Values with Experimental k_{eff} Values

	CA-1				CA-18			
	Leakage Fraction	Absorption Fraction	k_{eff}	Percent Thermal Fission	Leakage Fraction	Absorption Fraction	k_{eff}	Percent Thermal Fission
Calculations								
Method I	0.4583	0.5417	1.0215	4.32	0.4560	0.5439	1.0550	37.95
Method II	0.4655	0.5345	1.0102	8.07	0.4843	0.5157	0.9839	45.32
Method IIa	0.4651	0.5349	1.0110	8.08	-	-	-	-
Method III	0.5094	0.4906	0.9290	7.95	0.5202	0.4798	0.9153	45.10
Method IV	0.5074	0.4926	0.9323	6.14	0.5090	0.4910	0.9369	42.10
Method V	0.4911	0.5087	0.9632	6.19	0.4954	0.5046	0.9734	41.8
Method VI	0.4872	0.5128	0.9675	6.17	-	-	-	-
Method VII	0.5133	0.4865	0.9190	3.89	-	-	-	-
Experiment	-	-	1.0054	-	-	-	1.0020	-

Table 10. Changes in Values of k for CA-1 and CA-18 Caused by Variations in Calculational Methods

Variation	Δk CA-1	Δk CA-18
No correction for uranium self shielding to a P_0 correction (Method I to Method II)	-0.01133	-0.07118
P_0 correction for uranium self shielding to a P_1 correction (Method III to Method IV)	-0.00803	-0.04954
No inelastic scattering in U^{235} to inelastic scattering for energies above 1 Mev (Method II to Method IIa)	+0.00081	
Isotropic scattering in beryllium to anisotropic scattering for energies above 1 Mev (Method IIa to Method III)	-0.08120	-0.06858
No inelastic scattering in beryllium to inelastic scattering for energies above 1 Mev (Method IV to Method VI)	+0.03519	
$\phi \xi \Sigma_t$ slowing-down model to $\phi \xi \Sigma_s$ Fermi model (Method IV to Method VII)	+0.0133	
No correction for effect of aluminum grid to a correction (Method IV to Method V)	+0.03093	+0.03647

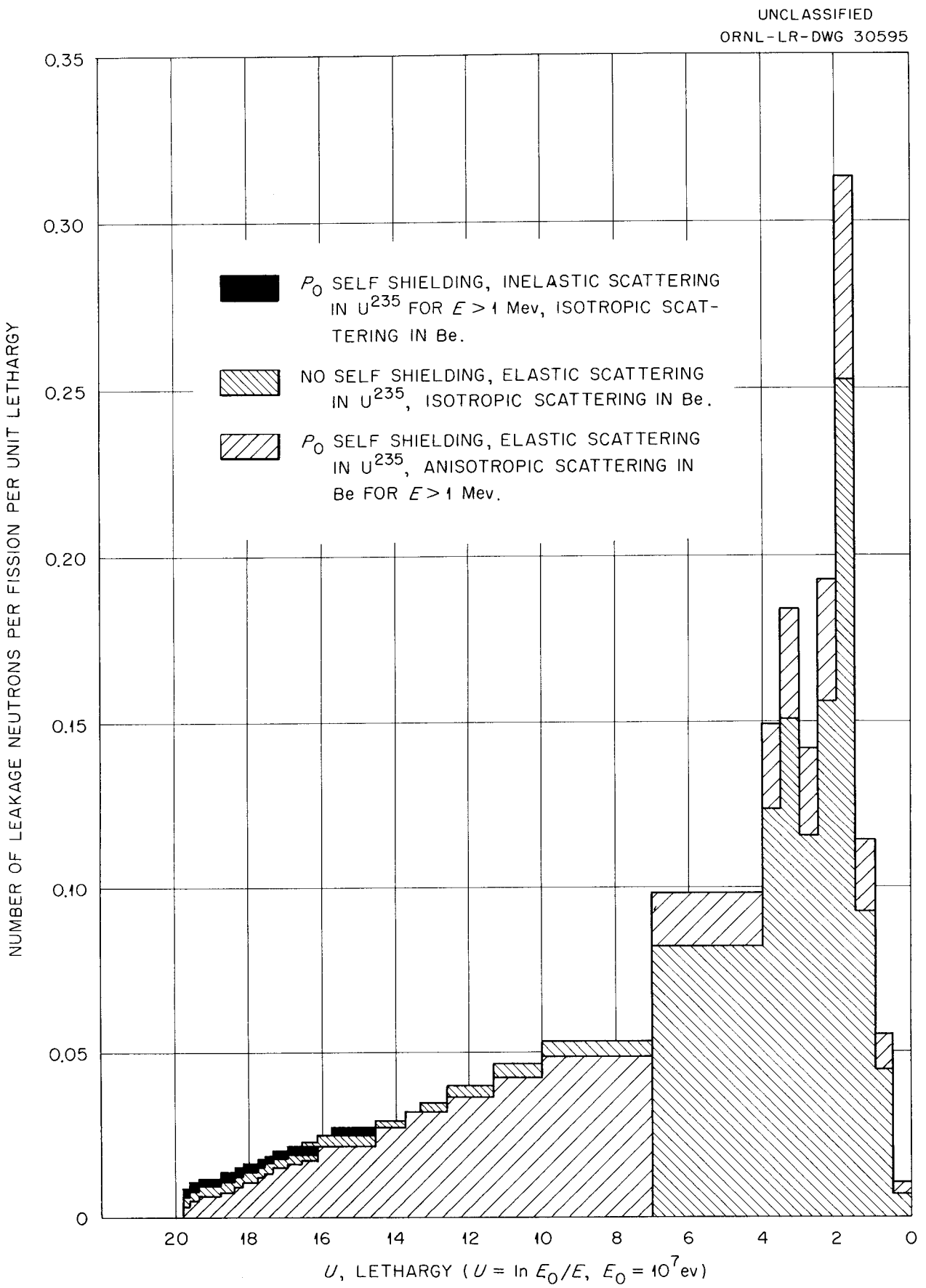

Fig. 15. Calculated Neutron Leakage Spectra for CA-1 for Various Assumptions and Corrections.

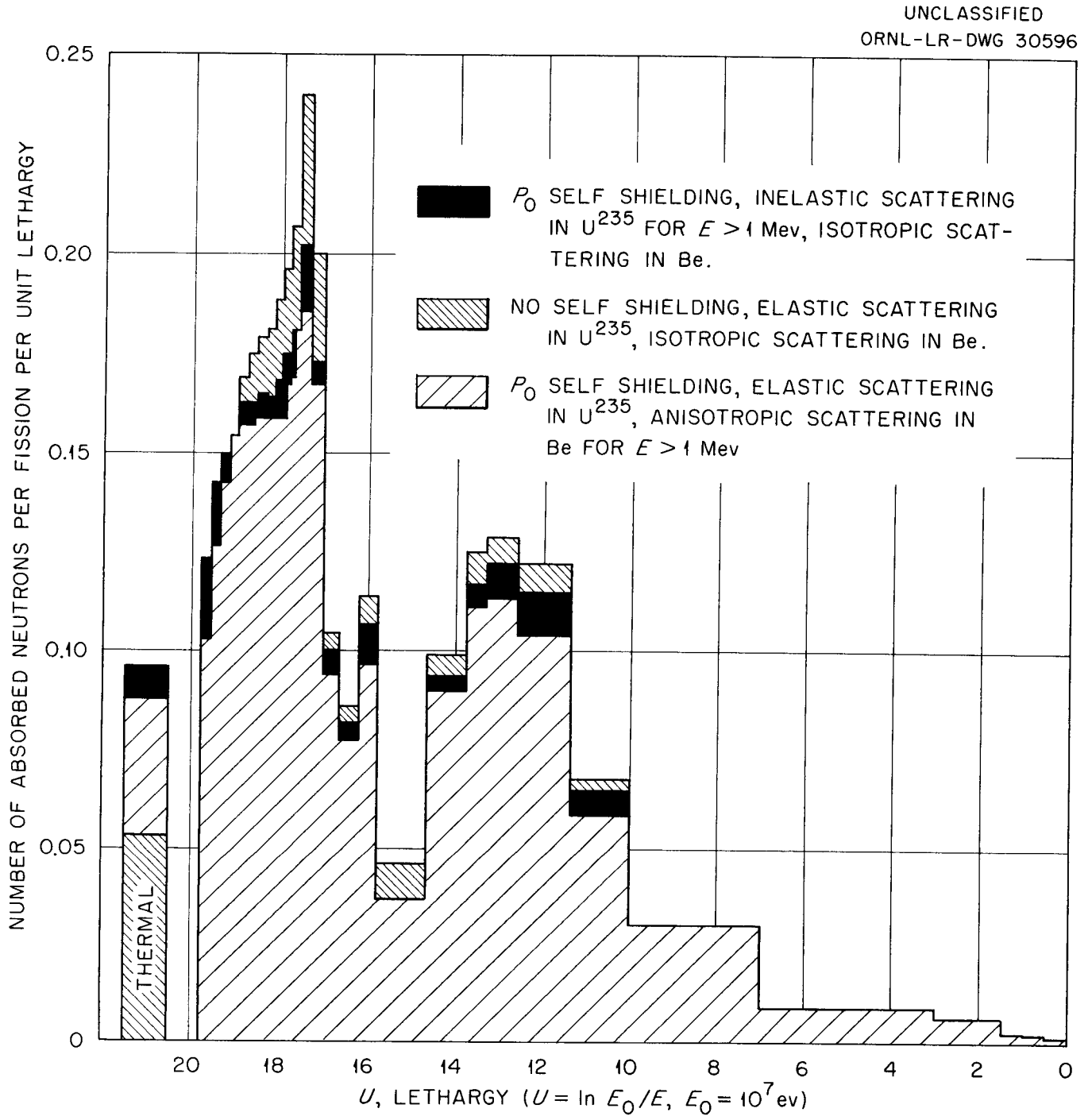

Fig. 16. Calculated Neutron Absorption Spectra for CA-1 for Various Assumptions and Corrections.

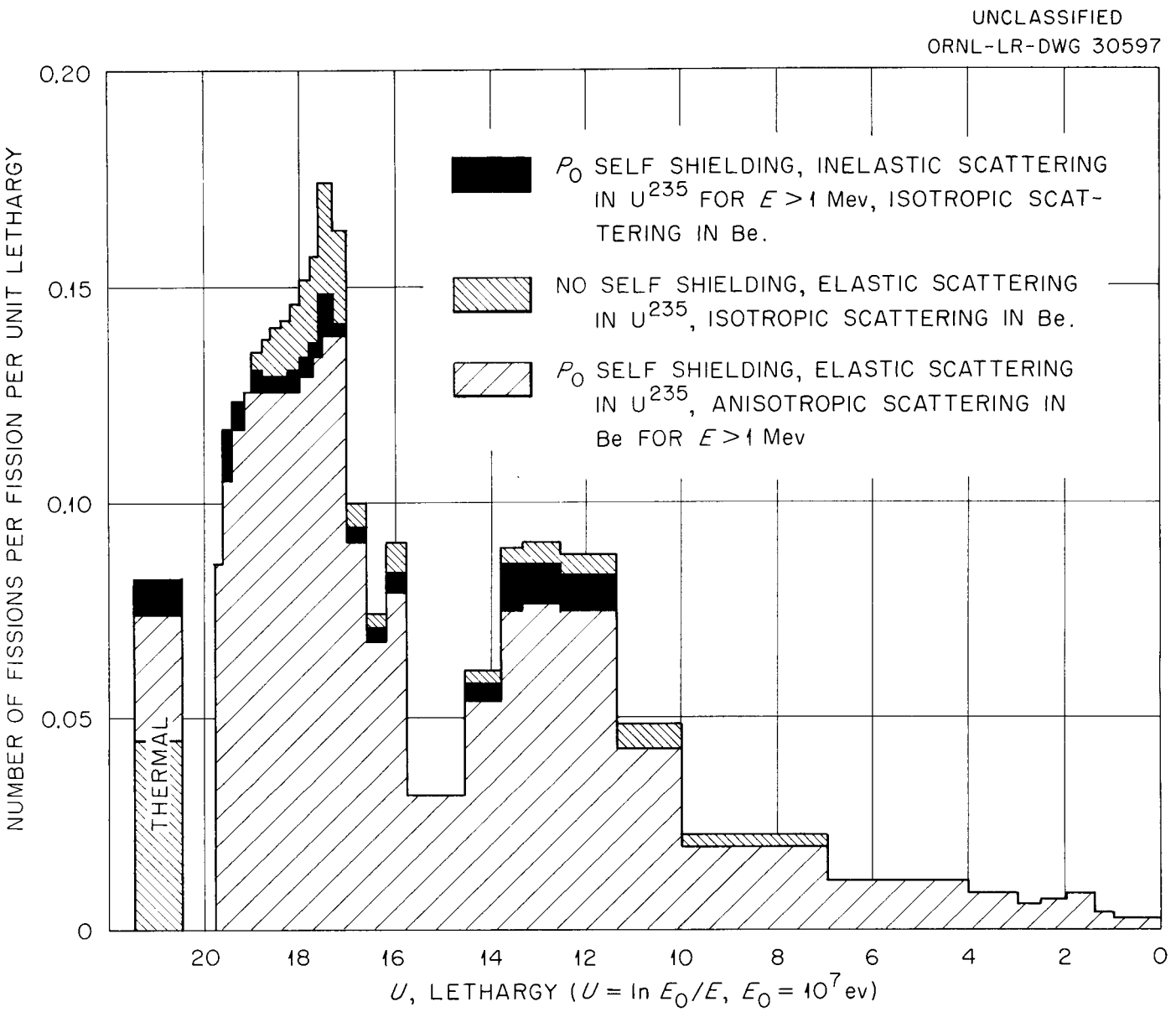

Fig. 17. Calculated Fission Spectra for CA-1 for Various Assumptions and Corrections.

Table 11. Comparison of Calculated Cadmium Fractions and Uranium Self-Shielding Factors with Experimental Values

	Cadmium Fractions			
	Fuel Disks		Indium Foils, CA-18	Self-Shielding Factor, CA-18
	CA-1	CA-18		
Calculations				
Method I		0.753	0.258	0.649
Method II	0.456	0.820	0.348	0.799
Method III		0.816	0.326	
Method IV		0.793	0.289	
Method V		0.793	0.292	0.847
Experiment	0.46	0.852-0.888	0.28-0.40	0.892

correction. This would imply a more thermal system than the calculations show and perhaps a self-shielding effect even greater than that indicated by the P_0 factors. One measurement of the cadmium fraction was made in CA-1, but the result is very approximate due to uncertainties in counting corrections available at that time.

An approximate method was used to calculate reactivity coefficients of poisons, but only in hopes of obtaining agreement to within an order of magnitude. Dependable self-shielding corrections are not available for the particular sizes of poison samples used. Further, a significant comparison could not be made without first calculating the complete adjoint flux corresponding to each of the multigroup calculations.

Comparison of Present Calculations for CA-1 with Previous Calculations

The method used in the original calculation[15] for CA-1 assumed the Fermi age form for the neutron slowing-down density but otherwise was similar to the second calculation reported here. The difference in k_{eff} primarily is due to differences in the high-energy scattering cross sections for beryllium which at that time were somewhat lower than values from more recent data.

15. A. O. Mooneyham, NEPA-1710, op. cit.

Following the experiment with CA-1, a number of other calculations[16] were made using a variety of assumptions and methods. Variations, such as using from 15 to 45 energy groups, assuming a monoenergetic 2-Mev fission neutron source instead of a fission neutron distribution, and varying the fuel self-shielding correction, gave only small changes in the calculated critical mass. However, it was found that a small increase in the scattering cross section for beryllium in the range 10^7 to 10^5 ev would give the correct value of critical mass. It was concluded that the calculations were very sensitive to high-energy scattering cross-section values, but were relatively insensitive to self-shielding corrections or the number of energy groups used.

In a later calculation[17] a correction for anisotropic scattering in beryllium was made in order to get a result for the age in agreement with the experimentally determined value. Several other corrections were made which were adequate to bring the calculation into agreement with the experimental size of CA-1. The agreement between this calculation and the experiment is considerably better than that found in the present set of calculations although it is somewhat artificial. As has been observed previously, k_{eff} is very sensitive to any change in high-energy data or any correction which effects the competition between high-energy leakage and slowing down. In the meantime, the same factors cause similar changes in calculated age. Mills did make a scattering correction in order to give the correct experimental age resulting in a decrease in k_{eff} of about 10%. The beryllium inelastic scattering correction approximately compensated k_{eff} for this loss, but its effect on age was not considered. In other words a consistent agreement with the experimental values of age and k_{eff} could not be found simultaneously.

This dilemma has not been resolved by the present investigation. Good agreement, however, may be found for k_{eff} by simply adjusting data in the high-energy range. While this is quite arbitrary, the choice may certainly be well within the range of uncertainty in fundamental data.

IV. CONCLUSIONS

The primary purpose of this report is to make available the experimental results obtained from the two beryllium-moderated critical assemblies. The multigroup calculations were made in an effort to evaluate some of the uncertainties involved and, if possible, to indicate an approach which would be applicable to other reactors. While it is possible by a judicious choice of data to get good agreement with the critical experiments, the rules governing the choice are certainly not clear.

An agreement in the value of k_{eff} does not in itself imply an understanding of the detailed neutron behavior. If, however, the critical size or critical mass of the system is the primary consideration, a fairly

16. G. M. Safanov, YF-10-45, op. cit.
17. C. B. Mills et al., ORNL-1493, op. cit.

dependable calculation may be made by adjusting high-energy fundamental data to give agreement with the critical experiments. A number of such quantities may be adjusted, namely, the value of the high-energy scattering cross section, the term for anisotropic scattering, inelastic scattering, etc. The critical size, or the actual k_{eff}, are convenient experimental quantities for a theoretical comparison since they may be observed accurately. Unfortunately, other available observed quantities are themselves subject to interpretations which involve uncertainties comparable to those in the multigroup calculations.

Appendix A

CALCULATION OF THE REACTIVITY VALUE OF A BERYLLIUM LAYER ON TOP OF CA-18

As stated in Section II, for the absolute calibration of the control rods in CA-18 it was necessary to determine the change in reactivity in the system effected by the addition of a 1/4-in.-thick layer of beryllium on the top of the assembly. The calculation was performed in the following manner. In a parallelepiped of augmented dimensions a x b x c, the geometric buckling of the system is

$$B_o^2 = \left(\frac{\pi}{a}\right)^2 + \left(\frac{\pi}{b}\right)^2 + \left(\frac{\pi}{c}\right)^2 \qquad (A.1)$$

If c is increased a small amount, δc, the buckling will be decreased an amount

$$\delta B^2 = -\left(\frac{\pi}{c}\right)\left(\frac{2\delta c}{c}\right) \qquad (A.2)$$

Assume that the multiplication k_{eff} may be written in the form

$$k_{eff} = AP_{nl} \qquad (A.3)$$

where A is a constant and P_{nl} is the nonleakage probability

$$P_{nl} = e^{-M^2 B_o^2} \qquad (A.4)$$

M^2 being the migration area. The change, δk, in k_{eff} found by substituting Eqs. A.2 and A.4 into A.3 is

$$k_{eff} + \delta k = Ae^{-M^2(B_o^2 + \delta B^2)}$$

and

$$\frac{\delta k}{k_{eff}} = M^2 \left(\frac{\pi}{c}\right)^2 \left(\frac{2\delta c}{c}\right) \qquad (A.5)$$

Solving Eq. A.4 for M^2 and substituting into Eq. A.5 gives:

$$\frac{\delta k}{k_{eff}} = \left(\frac{1}{B_o^2}\right)\left(\frac{\pi}{c}\right)^2 \left(\frac{2\delta c}{c}\right) \ln \frac{1}{P_{nl}} \qquad (A.6)$$

In Eq. A.6 the value of c is 73.89 cm which corresponds to one of the augmented dimensions in CA-18, and δc is 0.635 cm, which corresponds to the 1/4-in. thickness of beryllium. The values of B_o^2 and P_{nl} were obtained from a multigroup calculation as follows:

$$B_o^2 = 0.00655 \text{ cm}^{-2}$$
$$P_{nl} = 0.4765$$

Substituting these values in Eq. A.6 yields

$$\frac{k}{k_{eff}} = 0.003231.$$

Appendix B

MULTIGROUP FORMULATION*

For the multigroup formulation the neutron energy range is divided into n groups plus a thermal group. Lethargy is defined as $u \equiv \ln(E_o/E)$, where $E_o = 10^7$ ev and E is some particular neutron energy.

Consider group i in which u has the range $u_{i-1} \leq u \leq u_i$, and $U_i = u_i - u_{i-1}$. The fission source in group i, i.e., the number of neutrons born with energy i, is represented by νZ_i. Fission sources are normalized such that $\sum_{i=1}^{n} \nu Z_i = \nu$. The slowing-down density at a particular lethargy u is designated by q and the appropriate subscript. Cross sections are lethargy averages over each group and are considered as constant over the particular group. The probability that a neutron will slow down from u past u_i without loss due to absorption or leakage is given by

$$e^{-\frac{2C_i(u_i - u)}{U_i}}$$

where

$$C_i = \frac{(\Sigma_{ai} + DB_i^2)U_i}{2\xi_i \Sigma_{ti}} \tag{B.1}$$

where

Σ_a = absorption cross section,
DB^2 = leakage cross section,
D = diffusion coefficient,
B^2 = buckling,
ξ = average lethargy gain per neutron collision,
Σ_t = total cross section,
= $\Sigma_s + \Sigma_a + DB^2$,
Σ_s = scattering cross section.

In the Fermi age approximation, $\Sigma_t = \Sigma_s$.

The contribution of q_i from group i-1 is $q_{i-1}e^{-2C_i}$, while the contribution from the fission source is

$$\int_{u_{i-1}}^{u_i} \nu Z_i \frac{du}{U_i} e^{-\frac{2C_i(u_i - u)}{U_i}} = \frac{\nu Z_i}{2C_i}(1 - e^{-2C_i}) \tag{B.2}$$

The total contribution is

$$q_i = q_{i-1} e^{-2C_i} + \frac{\nu Z_i}{2C_i}(1 - e^{-2C_i})$$

---

* This is a conventional multigroup formulation included here for completeness of the report; see, for example, reference 6, p. 115.

$$= \frac{1}{e^{C_i}} \left[q_{i-1} e^{-C_i} + \frac{\nu Z_i}{2C_i} (e^{C_i} - e^{-C_i}) \right]$$

$$\cong \frac{q_{i-1} (1 - C_i) + \nu Z_i}{1 + C_i}$$

This is the recursion relation used in the multigroup calculations. If ϕ_i is the average flux in group i, then the losses by leakage and absorption are

$$E_i = \phi_i DB^2 U_i \text{ and } A_i = \phi_i \Sigma_{ai} U_i$$

respectively. The neutron balance for group i is given by

$$q_{i-1} + \nu Z_i = q_i + \phi_i U_i (\Sigma_{ai} + DB_i^2) \tag{B.3}$$

Solving Eq. B.3 for ϕ_i and using the definition of C_i,

$$\phi_i = \frac{\bar{q}_i}{\xi_i \Sigma_{ti}} \tag{B.4}$$

where

$$\bar{q}_i = \frac{q_{i-1} + q_i}{2}$$

The thermal-neutron flux is given by

$$\phi_{th} = \frac{q_n}{(\Sigma_a^{th} + DB_{th}^2)} \tag{B.5}$$

The fission rate in group i is $F_i = \phi_i \Sigma_{fi} U_i$ where Σ_f is the fission cross section. The criticality equation is

$$\sum_{i=1}^{n} F_i + F_{th} = 1 \tag{B.6}$$

Inelastic scattering is included in the calculation by adding the neutrons scattered into a particular group to the fission source term in that group. The definition of C_i in Eq. B.1 is changed to include the inelastic scattering cross section by adding the inelastic cross section to the term in parentheses.

Appendix C

SOURCE DISTRIBUTION AND CORRESPONDING CROSS-SECTION DATA FOR THE REACTOR MATERIALS

Group				Microscopic Cross Sections (barns)						Stainless Steel Macroscopic Scattering Cross Section[c] (cm^{-1})
				Enriched Uranium			Beryllium	Aluminum		
Number	Upper Lethargy Limit $u_0=0$	Lower Energy Limit (ev) ($E_0=10^7$ ev)	νZ_i, Number of Neutrons[a]	σ_s	σ_a	σ_f	σ_s	σ_s	σ_a	
1	0.5	6.06×10^6	0.0525	3.5	1.25	1.18	1.7	1.8	0.0001	0.269
2	1.0	3.68×10^6	0.2600	3.7	1.24	1.17	1.9	2.3	0.0002	0.303
3	1.5	2.23×10^6	0.5175	4.3	1.23	1.16	2.4	2.9	0.00035	0.252
4	2.0	1.35×10^6	0.5775	4.2	1.22	1.15	1.9	3.0	0.00038	0.235
5	2.5	0.82×10^5	0.4575	4.8	1.21	1.13	3.1	3.1	0.00038	0.201
6	3.0	4.98×10^5	0.2925	6.0	1.26	1.18	4.0	3.5	0.0006	0.201
7	3.5	3.02×10^5	0.1675	7.2	1.41	1.26	3.7	4.0	0.0004	0.294
8	4.0	1.83×10^5	0.0875	7.8	1.63	1.40	4.2	4.0	0.0014	0.300
9	7.0	9.12×10^3	0.0875	9.4	2.78	2.26	5.1	4.0	0.0030	0.350
10	10.0	4.54×10^2	0	10.5	8.88	6.23	6.0	1.35	0.0009	0.570
11	11.4	1.12×10^2	0	15	22.3	15.60	6.0	1.35	0.0016	0.770
12	12.6	3.372×10^1	0	12	47.0	33.4	6.0	1.35	0.0043	0.880
13	13.4	1.515×10^1	0	9.5	58.1	40.3	6.0	1.35	Assume 1/v	0.880
14	13.8	1.015×10^1	0	9.0	61.4	43.8	6.0	1.35	"	0.880
15	14.6	4.546	0	8.5	52.9	32.7	6.0	1.35	"	0.880
16	15.8	1.375	0	8.5	26.3	18.7	6.0	1.35	"	0.880
17	16.2	9.214×10^{-1}	0	8.5	76.5	60.1	6.0	1.35	"	0.880
18	16.6	6.176×10^{-1}	0	8.5	60.6	52.5	6.0	1.35	"	0.880
19	17.0	4.140×10^{-1}	0	8.5	78.3	74.4	5.8	1.35	"	0.880
20	17.4	2.775×10^{-1}	0	8.5	172.	143.5	5.7	1.35	"	0.880
21	17.6	2.275×10^{-1}	0	8.5	242.	179.3	5.6	1.35	"	0.880
22	17.8	1.860×10^{-1}	0	8.5	227.	174.6	5.5	1.35	"	0.880
23	18.0	1.523×10^{-1}	0	8.5	237.	184.7	5.4	1.35	"	0.880
24	18.2	1.247×10^{-1}	0	8.5	253	198.9	5.3	1.35	"	0.880
25	18.4	1.021×10^{-1}	0	8.5	273	216.7	5.2	1.35	"	0.880
26	18.6	8.36×10^{-2}	0	8.5	305	241.9	5.0	1.35	"	0.880
27	18.8	6.843×10^{-2}	0	8.5	342	273.6	4.8	1.35	"	0.880
28	19.0	5.603×10^{-2}	0	8.5	386	311	4.5	1.35	"	0.880
29	19.2	4.587×10^{-2}	0	8.5	426	349.3	4.3	1.35	"	0.880
30	19.4	3.756×10^{-2}	0	8.5	475	393.2	3.9	1.35	"	0.880
31	19.6	3.075×10^{-2}	0	8.5	530	441.8	3.5	1.35	"	0.880
32	19.8	2.518×10^{-2}	0	8.5	590	495.0	3.4	1.35	"	0.880
Th	19.8	2.518×10^{-2}	0	1	636	537.1	3[b]	1.35	0.215	0.880

a. νZ_i = number of fission neutrons born in the ith energy group.

b. σ_a^{th} = 0.009 barn; assume $1/v$ for higher energy groups.

c. Σ_a^{th} = 0.240 cm^{-1}; " " " " " .

Appendix D

CALCULATIONS OF SELF-SHIELDING CORRECTIONS*

In a system in which the flux $\phi(x)$ is a function of a single cartesian coordinate x, diffusion theory gives the following expression for differential flux and current:

$$F(x,\mu) = \frac{\phi(x)}{2} - \frac{3D}{2}\phi'(x)\mu$$

$$G(x,\mu) = \frac{\phi(x)}{2}\mu - \frac{3D}{2}\phi'(x)\mu^2 \qquad \text{(D.1)}$$

Here μ is the cosine of the angle between the neutron direction and the x axis. Integrating the terms in Eq. D.1 over all directions gives for the total flux

$$\int_{-1}^{1} F(x,\mu)d\mu = \phi(x)$$

and for the net current

$$\int_{-1}^{1} G(x,\mu)d\mu = -D\phi'(x) = J(x)$$

An infinite plane absorber of thickness t having absorption cross section Σ_a is placed in the medium normal to the x axis. A neutron at x = 0 traveling in a direction μ has the probability $e^{-\Sigma_a t/\mu}$ of passing through the absorber. Then

$$G(x + t,\mu) = G(x,\mu)e^{-\Sigma_a t/\mu} \qquad \text{(D.2)}$$

The partial current of neutrons having a component of motion in the positive x direction is

*This approximation was derived by J. H. Marable, ORNL.

$$j_+(x + t) = \int_0^1 G(x + t,\mu)d\mu = \int_0^1 G(x,\mu)e^{-\Sigma_a t/\mu} d\mu$$

$$= \frac{\phi(x + t)}{4} - \frac{D}{2}\phi'(x + t) = \frac{\phi(x)}{4} f_1(\Sigma_a t) - \frac{D}{2}\phi'(x)f_2(\Sigma_a t) \qquad (D.3)$$

where

$$f_n(\Sigma_a t) = (n + 1) \int_0^1 \mu^n e^{-\Sigma_a t/\mu} d\mu \qquad (D.4)$$

Similarly

$$j_-(x) = \frac{-\phi(x)}{4} - \frac{D}{2}\phi'(x) = -\frac{\phi(x + t)}{4} f_1(\Sigma_a t) - \frac{D}{2}\phi'(x + t)f_2(\Sigma_a t) \qquad (D.5)$$

In the following, the argument of $f_1(\Sigma_a t)$ and $f_2(\Sigma_a t)$ are dropped for simplicity in notation . From Eqs. D.3 and D.5 the derivatives of flux are

$$\frac{D}{2}\phi'(x + t) = \frac{(1 + f_1 f_2)\,\phi(x + t)/4 - (f_1 + f_2)\,\phi(x)/4}{(1 - f_2^2)}$$

$$\frac{D}{2}\phi'(x) = \frac{-(1 + f_1 f_2)\,\phi(x)/4 + (f_1 f_2)\,\phi(x + t)/4}{(1 - f_2^2)}$$

The absorption rate per unit area in the element dp at depth p in the absorber is $\phi(x + p)\Sigma_a dp$. The absorption rate of neutrons entering the absorber from the left is

$$N_x = \int_0^t \phi_x(x + p)\Sigma_a dp = \Sigma_a \int_0^t dp \int_0^1 F(x + p,\mu)d\mu = \Sigma_a \int_0^t \int_0^1 F(x,\mu)e^{-\Sigma_p/\mu} d\mu dp$$

$$= \Sigma_a \int_0^1 \phi(x,\mu)\frac{\mu}{\Sigma_a}(1 - e^{-\Sigma_a t/\mu})d\mu = \int_0^1 \left[\frac{\phi(x)}{2} - \frac{3D}{2}\phi'(x)\mu\right](1 - e^{-\Sigma_a t/\mu})\mu d\mu$$

$$= \frac{\phi(x)}{4}(1 - f_1) - \frac{D\phi'(x)}{2}(1 - f_2) \qquad \text{(D.7a)}$$

Similarly, the absorption rate of neutrons entering from the right is

$$N_{x+t} = \frac{\phi(x + t)}{4}(1 - f_1) + \frac{D\phi'(x + t)}{2}(1 - f_2) \qquad \text{(D.7b)}$$

The total absorption rate is the sum,

$$N = \frac{(1 - f_1)}{2}\frac{\phi(x) + \phi(x + t)}{2} - (1 - f_2)\frac{D}{2}\left[\phi'(x) - \phi'(x + t)\right] \qquad \text{(D.7c)}$$

Substituting the expressions from Eq. D.6 into D.7c gives the absorption rate

$$N = \left(\frac{1 - f_1}{1 + f_2}\right)\left(\frac{\phi(x) + \phi(x + t)}{2}\right) = \left(\frac{1 - f_1}{1 + f_2}\right)\bar{\phi} \qquad \text{(D.8)}$$

where $\bar{\phi}$ is the average of the two boundary values of the flux. Assuming no self shielding, the absorption rate would be $N_o = \bar{\phi}\Sigma_a t$. The self-shielding factor is therefore the ratio

$$S_1 = \frac{1}{\Sigma_a t\bar{\phi}}\left(\frac{1 - f_1}{1 + f_2}\right)\bar{\phi} = \frac{1}{\Sigma_a t}\left(\frac{1 - f_1}{1 + f_2}\right) \qquad \text{(D.9)}$$

This is the p_1 self-shielding factor and may be compared to p_o approximation which has the form

$$S_o = \frac{1}{\Sigma_a t}\left(\frac{1 - f_1}{2}\right) \tag{D.10}$$

The functions S_1 and S_2 are shown in Fig. 14, p. 27 .

A similar approach has been used to calculate the activation rate of a foil covered on both sides by similar absorbers. Using the notation $x = \Sigma_a t$ with subscript c for the covers and d for the detector foil, the activation rate of the detector per unit area per unit time is

$$N = \bar{\phi}\,\frac{f_1(x_c) - f_1(x_c + x_o)}{2} + \frac{\left[1 - f_1(x_d + 2x_c)\right]\left[f_2(x_c) - f_2(x_d + x_c)\right]}{2\left[1 + f_2(x_d + 2x_c)\right]} \tag{D.11}$$

Consider the function $f_n(x) \equiv (n + 1)\int_0^1 \mu^n e^{-x/\mu} d\mu$ given in Eq. D.4.

Direct partial integration gives the recursion relation

$$f_n(x) = -\frac{x}{n} f_{n-1}(x) + e^{-x} \tag{D.12}$$

Also note that[1]

$$f_o(x) = \int_0^1 e^{-x/\mu} d\mu = e^{-x} + xEi(-x) \tag{D.13}$$

By Eqs. D.12 and D.13

$$\left.\begin{aligned} f_o(x) &= e^{-x} + xEi(-x) \\ f_1(x) &= (1 - x)e^{-x} - x^2 Ei(-x) \\ f_2(x) &= \left(1 - \frac{x(1 - x)}{2}\right) e^{-x} + \frac{x^3}{2} Ei(-x) \end{aligned}\right\} \tag{D.14}$$

1. The function of $-Ei(-x) \equiv \int_x^\infty \frac{e^{-t}}{t} dt$ is the exponential integral, the values of which are tabulated. See, for example, "Table of Functions," by Jahnke and Emde, Dover Publications (1945).

The function f (x) is related to the tabulated function[2]

$$E_n(x) \equiv \int_1^\infty e^{-x\mu}\mu^{-n}d\mu$$

by

$$E_n(x) = \frac{f_{n-2}(x)}{n - 1} \tag{D.15}$$

or

$$f_n(x) = (n + 1)E_{n+2}(x).$$

2. G. Placzek, "The Functions $E_n(x) \equiv \int_1^\infty e^{-x\mu}\mu^{-n}d\mu$," MT-1.

Appendix E

CALCULATIONS OF ξ FOR ANISOTROPIC SCATTERING

Consider a neutron of energy E, which is elastically scattered by a nucleus of atomic mass A. Defining μ as the cosine of the scattering angle in the center of mass system, the energy, E_2, of the neutron after collision is given by

$$E_2 = E_1\left[\left(\frac{1+\alpha}{2}\right) + \left(\frac{1-\alpha}{2}\right)\mu\right] \tag{E.1}$$

where $\alpha \equiv \left(\frac{A-1}{A+1}\right)^2$.

In isotropic scattering the frequency function for scattering into a range $d\mu$ about μ is given by

$$f_o(\mu) = \frac{1}{2}, \quad \text{which satisfies the normalization} \quad \int_{-1}^{1} f_o(\mu)d\mu = 1. \tag{E.2}$$

The average μ is zero in this case.

In anisotropic scattering one has a frequency function

$$f(\mu) = f_o(\mu) + f_1(\mu) = \frac{1}{2} + f_1(\mu).$$

Normalization requires that $\int_{-1}^{1} f_1(\mu)d\mu = 0$ (E.3)

The average cosine, $\bar{\mu}$, may be measured experimentally and is given by

$$\bar{\mu} = \int_{-1}^{1} \mu f(\mu)d\mu = \int_{-1}^{1} \mu f_1(\mu)d\mu. \tag{E.4}$$

The average lethargy gain per collision, ξ, may be calculated immediately.

$$\xi \equiv \overline{\ln \frac{E_1}{E_2}} = \int_{-1}^{1} \left(\ln \frac{E_1}{E_2}\right) f(\mu)d\mu = \int_{-1}^{1} \ln \frac{E_1}{E_2} \left[f_o(\mu) + f_1(\mu)\right] d\mu$$

$$= - \int_{-1}^{1} \ln \left(\frac{1+\alpha}{2} + \frac{1-\alpha}{2}\mu\right) \left(\frac{1}{2}\right) d\mu - \int_{-1}^{1} \ln \left(\frac{1+\alpha}{2} + \frac{1-\alpha}{2}\mu\right) f_1(\mu)d\mu$$

$$= \xi_o - \int_{-1}^{1} \left[\ln \left(\frac{1+\alpha}{2}\right) + \ln \left(1 + \frac{1-\alpha}{1+\alpha}\mu\right)\right] f_1(\mu)d\mu$$

$$= \xi_o - \ln \left(\frac{1+\alpha}{2}\right) \int_{-1}^{1} f_1(\mu)d\mu - \int_{-1}^{1} \left[\frac{1-\alpha}{1+\alpha}\mu - \frac{1}{2}\left(\frac{1-\alpha}{1+\alpha}\right)^2 \mu + \ldots\right] f_1(\mu)d\mu$$

$$= \xi_o - \frac{1-\alpha}{1+\alpha} \int_{-1}^{1} \mu f_1(\mu)d\mu + \frac{1}{2}\left(\frac{1-\alpha}{1+\alpha}\right)^2 \int_{-1}^{1} \mu^2 f_1(\mu)d\mu + \ldots.$$

and finally

$$\xi \cong \xi_o - \frac{1-\alpha}{1+\alpha}\bar{\mu}, \tag{E.5}$$

using Eqs. E.3 and E.4 and ignoring higher order terms in $\left(\frac{1-\alpha}{1+\alpha}\right)$. ξ_o is the value of ξ for the isotropic scattering case. The approximation is convenient if $\bar{\mu}$ is known experimentally. Ignoring higher order terms in $\left(\frac{1-\alpha}{1+\alpha}\right)$ is not serious for heavy elements, e.g., in the case of beryllium where A = 9, $\frac{1}{2}\left(\frac{1-\alpha}{1+\alpha}\right)^2 = 0.024$ compared to $\left(\frac{1-\alpha}{1+\alpha}\right) = 0.22$. Using the value of $\bar{\mu}$ from page 28 the value of ξ is found to be $0.206 - (0.220)(0.254) = 0.150$.

Appendix F

CORRECTION FOR EXTERNAL ALUMINUM GRID

Consider a spherical reactor having a core radius r and an outside reflector radius R. The reflector is nonabsorbing material having a scattering mean free path

$$\lambda_s = \frac{1}{\Sigma_s} > R - r.$$

A fraction of the neutrons leaking out of the core will undergo collisions in the reflector and may eventually be returned to the core. Only first collisions are considered in this approximation. From Fig. F-1a

$$\rho = r\left[\left(\frac{R^2 - r^2}{r^2} + \mu^2\right)^{1/2} - \mu\right] \qquad (F.1)$$

where $\mu = \cos\theta$.

Assuming the leakage to be constant in μ, the average of ρ is found to be

$$\bar{\rho} = \frac{\int_0^1 \rho d\mu}{\int_0^1 d\mu} = \frac{R - r}{2} + \frac{R^2 - r^2}{4r} \ln\left(\frac{R + r}{R - r}\right) \qquad (F.2)$$

If the total leakage rate from the core is E, the number of first collisions per unit time in the reflector will be $n = E\Sigma_s\bar{\rho}$. (F.3)

Assuming the first-collision density to have an inverse square distribution, the first-collision density in a volume element $x^2 d\Omega dx$ (see Fig. F-1b), is

$$\frac{n dx d\Omega}{4\pi(R - r)} \qquad (F.4)$$

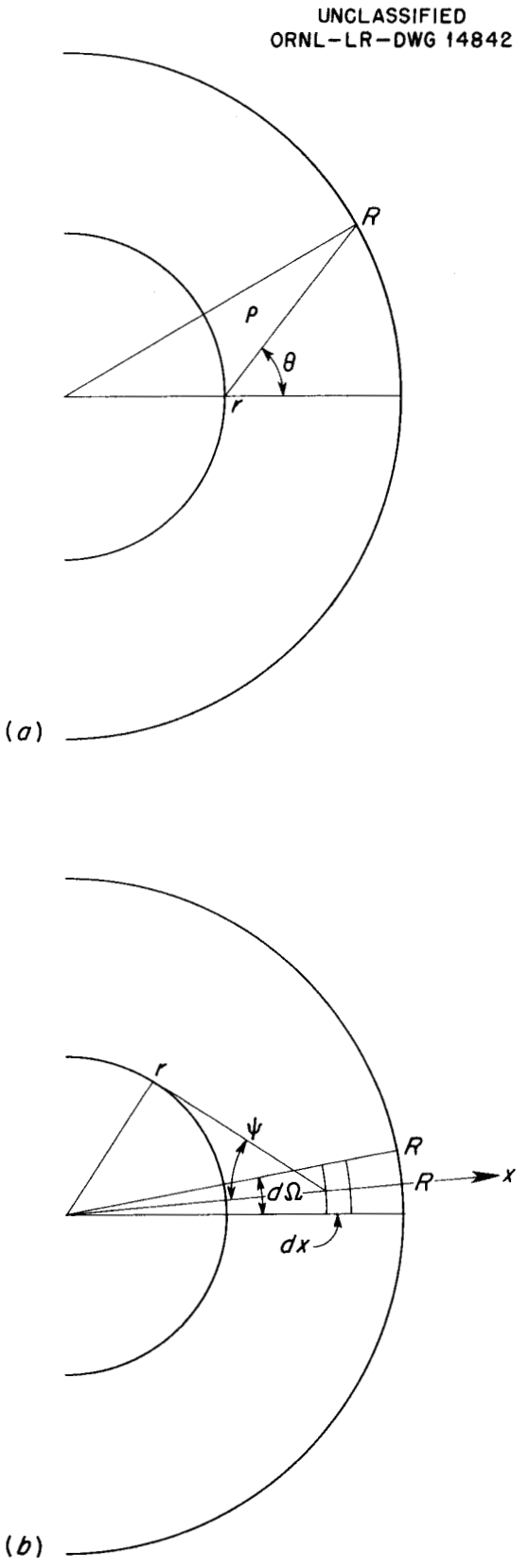

Fig. F-1. Spherical Reactor Geometry for Calculation of Leakage Correction Which Includes Effect of Aluminum Grid.

The fraction of solid angle subtended by the core at a distance x is

$$\frac{1 - \cos\psi}{2} = \frac{1}{2}\left[1 - \frac{(x^2 - r^2)^{1/2}}{x}\right]. \tag{F.5}$$

Assuming isotropic scattering and combining Eqs. F.3, F.4, and F.5 the rate of return to the core is

$$F = \int_{x=r}^{R} \int_{\Omega} \left(\frac{1}{2}\right)\left(1 - \frac{(x^2 - r^2)^{1/2}}{x}\right)\left(\frac{n\,dx\,d\Omega}{4\pi(R - r)}\right)$$

$$= \frac{E\Sigma_s}{4}\left(1 + \frac{R + r}{2r} \ln \frac{R + r}{R - r}\right)\left[(R - r) - (R^2 - r^2)^{1/2} + r \cos^{-1} \frac{r}{R}\right] \tag{F.6}$$

and the fraction of leakage neutrons which are returned is

$$f = \frac{F}{E} = \frac{\Sigma_s}{4}\left[1 + \frac{R + r}{2r} \ln \frac{R + r}{R - r}\right]\left[(R - r) - (R^2 - r^2)^{1/2} + r \cos^{-1} \frac{r}{R}\right] \tag{F.7}$$

Neutrons which reenter the core are assumed to be distributed uniformly throughout the core and are less effective than the same number of neutrons would be in a normal distribution.

In a parallelpiped bare reactor of dimension 2a x 2b x 2c, the flux is given by

$$\phi(x,y,z) = \phi_o \cos \frac{x\pi}{2a} \cos \frac{y\pi}{2b} \cos \frac{z\pi}{2c}. \tag{F.8}$$

In the normal mode the source density is given by

$$q(x,y,z) = q_o \left(\cos \frac{x\pi}{2a}\right)\left(\cos \frac{y\pi}{2b}\right)\left(\cos \frac{z\pi}{2c}\right), \tag{F.9}$$

where the total source, Q is $q_o \frac{8V}{\pi^3}$, and V is the volume of the reactor. In a uniform distribution the same number of neutrons would give rise to a source density $\bar{q} = \frac{Q}{V} = \frac{8}{\pi^3} q_o$.

Assuming the importance function for a source to be proportional to the flux, the relative effectiveness of a uniform distribution compared to that for a normal mode distribution is:

$$\frac{\text{I uniform}}{\text{I normal}} = \frac{\int_{vol} \bar{q}\phi(x,y,z)dv}{\int_{vol} \bar{q}(x,y,z)\phi(x,y,z)dv} = \left(\frac{8}{\pi^2}\right)^3 = 0.53256 \qquad \text{(F.10)}$$

Comparing CA-1 and CA-18 to a volume equivalent spherical system, one finds from Eqs. F.7 and F.10 the value of the effective f, i.e., the leakage correction discussed in Eq. F.7:

	CA-1	CA-18
r	34.22 cm	40.60 cm
R	134.5 cm	134.5 cm
f	8.646 Σ_s	9.960 Σ_s
Effective f	4.605 Σ_s	5.304 Σ_s

Appendix G

LIST OF FIGURES

Fig. No.		Page No.
1.	Midplane of CA-1	3
2.	Arrangement of Core Elements in CA-1 (Fixed Half Interface).	4
3.	Arrangement of Core Elements in CA-18 (Fixed Half Interface)	5
4.	Calibration of Control Rod C in CA-1	8
5.	Power Distribution Along a Lateral Axis in CA-1 (Gamma-Ray Activity of Uranium Disks)	11
6.	Power Distribution Along Several Longitudinal Traverses in CA-1 (Gamma-Ray Activity of Uranium Disks)	12
7.	Change in Reactivity of CA-18 as a Function of Withdrawal of Control Rods	14
8.	Calibration Curves for Control Rods in CA-18	15
9.	Activation of Indium Foils Along a Horizontal Lateral Traverse (1/4 in. from Midplane) in CA-18	18
10.	Activation of Indium Foils Along the Longitudinal Axis of CA-18	19
11.	Power Distribution Along a Lateral Axis of CA-18 (Fission Rate of Fuel Disks)	20
12.	Power Distribution Along the Longitudinal Axis of CA-18 (Fission Rate of Fuel Disks).	21
13.	Self-Shielding Factor for a 10-mil-Thick Fuel Disk in CA-18	22
14.	Uranium Self-Shielding Factors Calculated by P_0 and P_1 Approximations	27
15.	Calculated Neutron Leakage Spectra for CA-1 for Various Assumptions and Corrections	34

List of Figures (cont.)

Fig. No. Page No.

16. Calculated Neutron Absorption Spectra for CA-1 for Various Assumptions and Corrections 35

17. Calculated Fission Spectra for CA-1 for Various Assumptions and Corrections 36

F1. Spherical Reactor Geometry for Calculation of Leakage Correction Which Includes Effect of Aluminum Grid . . 53

Appendix H

LIST OF TABLES

Table No.		Page No.
1.	Comparative Descriptions of CA-1 and CA-18	6
2.	Effect of Various Surrounding Materials on the Reactivity of CA-1.	9
3.	Comparison of Reactivity Values of Control Rods in CA-18 Determined by Pile Period and by Absolute Calibration Methods	16
4.	Comparison of Reactivity Values of Control Rods in CA-18 Determined by Rod Drop and Absolute Calibration Methods.	16
5.	Reactivity Values of Various Materials Inserted in Cell K-13 Near the Center of CA-18	23
6.	Reactivity Values of Various Materials Inserted in Cell L-15 Near the Center of CA-18	23
7.	Reactivity Value of Fuel in CA-18	24
8.	Description of the Various Calculations	26
9.	Summary of Results of Multigroup Calculations for CA-1 and CA-18: Comparison of Calculated k_{eff} Values with Experimental k_{eff} Values	32
10.	Changes in Values of k for CA-1 and CA-18 Caused by Variations in Calculational Methods	33
11.	Comparison of Calculated Cadmium Fractions and Uranium Self-Shielding Factors with Experimental Values . . .	37

INTERNAL DISTRIBUTION

1. C. E. Center
2. Biology Library
3. Health Physics Library
4-5. Central Research Library
6. Reactor Experimental Engineering Library
7-26. Laboratory Records Department
27. Laboratory Records, ORNL R.C.
28. A. M. Weinberg
29. L. B. Emlet (K-25)
30. J. P. Murray (Y-12)
31. J. A. Swartout
32. E. H. Taylor
33. E. D. Shipley
34. A. H. Snell
35. E. P. Blizard
36. M. L. Nelson
37. W. H. Jordan
38. R. A. Charpie
39. S. C. Lind
40. F. L. Culler
41. A. Hollaender
42. J. H. Frye, Jr.
43. M. T. Kelley
44. J. L. Fowler
45. R. S. Livingston
46. K. Z. Morgan
47. T. A. Lincoln
48. A. S. Householder
49. C. P. Keim
50. C. S. Harrill
51. C. E. Winters
52. D. S. Billington
53. H. E. Seagren
54. D. Phillips
55. A. J. Miller
56. M. J. Skinner
57. R. R. Dickison
58. J. A. Harvey
59. A. Simon
60. F. C. Maienschein
61. C. E. Clifford
62. A. D. Callihan
63. R. R. Coveyou
64. W. Zobel
65. F. L. Keller
66. C. D. Zerby
67. D. K. Trubey
68. S. K. Penny
69. R. W. Peelle
70. F. Alsmiller
71. L. Dresner
72. W. K. Ergen
73. E. B. Johnson
74. P. Kasten
75. D. W. Magnuson
76. J. H. Marable
77. D. Scott
78. G. T. Chapman
79. G. deSaussure
80. R. Gwin
81. L. Jung
82. J. T. Mihalczo
83. A. M. Perry
84. E. G. Silver
85. J. T. Thomas
86. F. L. Friedman (consultant)
87. H. Goldstein (consultant)
88. H. Hurwitz, Jr. (consultant)
89. L. W. Nordheim (consultant)
90. R. R. Wilson (consultant)
91. ORNL - Y-12 Technical Library, Document Reference Section

EXTERNAL DISTRIBUTION

92. Frank Bly, Lockheed Aircraft Company, Marietta, Georgia
93. James Carothers, University of California Radiation Laboratory, Livermore
94. J. F. Coneybear, ASTRA Associates, Milford, Connecticut
95. Kenneth Downes, Brookhaven National Laboratory
96. John Flora, Atomics International, North American Aviation, Canoga Park, California

97. E. V. Haake, Convair, Fort Worth
98. J. A. Hunter, The Martin Company, Baltimore, Maryland
99. Edward Kuhn, Reactor Design Development Division, Combustion Engineering
100. C. B. Mills, Los Alamos Scientific Laboratory
101. A. O. Mooneyham, Convair Fort Worth
102. J. W. Noaks, Alco Products, Inc., Schenectady, N.Y.
103. H. C. Paxton, Los Alamos Scientific Laboratory
104. George Safanov, Rand Corporation, Santa Monica, California
105. D. V. P. Williams, Babcock and Wilcox. Lynchburg, Virginia
106-108. E. L. Zimmerman, Nuclear Development Corporation of America, White Plains, N.Y.
109. Division of Research and Development, AEC, ORO
110-656. Given distribution as shown in TID-4500 (13th ed., Rev.) under Criticality Studies category (75 copies - OTS)